Mode conversion of torsional guided waves for pipe inspection:

an electromagnetic acoustic transducer technique

Nurmalia

September 2013

Mode conversion of torsional guided waves for pipe inspection:

an electromagnetic acoustic transducer technique

A dissertation submitted to
THE GRADUATE SCHOOL OF ENGINEERING SCIENCE
OSAKA UNIVERSITY
in partial fulfillment of the requirements for the degree of
DOCTOR OF PHILOSOPHY IN ENGINEERING

Nurmalia

September 2013

ABSTRACT

The extensive usage of pipe structures in many high-risk industrial applications encourages the continual study of pipe inspection techniques. This study is motivated by the importance of defect detection and wall-thinning inspection in a pipe structures, that is, a frequent mechanism of pipe rupture. An electromagnetic acoustic transducer (EMAT) system with an original configuration is developed for this purpose. This is an entirely non-contact transducer, enabling measurement at high temperatures, less physical site preparation needed prior to inspection, and reduced time required for inspection itself. Torsional guided waves are utilized as a means for this inspection. A novel inspection method is proposed, which is based on group velocity change induced by mode conversion. This method relies on traveling time measurements, which is less susceptible to many factors, in contrast with the commonly-adopted amplitude based measurements. The group velocity of each higher torsional mode depends on pipe wall-thickness and its tendency to convert to a lower mode with a higher group velocity when the thickness is smaller than a critical value, the so-called cut-off thickness. The mode conversion behavior can then be a basis for pipe wall-thinning inspection.

Extensive fundamental studies are performed to explore the propagation and conversion behavior of torsional guided waves. The results of this study would provide a better understanding of the mode conversion phenomena. The fundamental torsional mode, T(0,1), and the first higher mode, T(0,2), are generated in pipes containing defects and their mode conversion behaviors are investigated. The conversion of T(0,2) mode to T(0,1) mode with a higher group velocity at the defect is observed. This conversion causes a decrease in traveling time which can be a basis for defect detection and characterization. It is also confirmed that the conversion behavior is sensitive to the shape of the thickness transition at the defect edge. Total reflection of the T(0,2) mode occurs in a pipe with a greatly-tapered defect.

The proposed method is then applied for inspection of various defects. Partial-circumferential defects are successfully detected by the proposed method. The method can detect a fully-circumference defect with an axial length as narrow as the generated wavelength. A system of two identical EMATs connected by a rod-shaft is also developed to enable internal inspection of pipe structures. This system successfully evaluates the presence of a dish-shaped defect. A scanning inspection of multiple defects is also demonstrated to simulate a practical application. A phase-shift is observed in response to the presence of a defect during the scanning.

TABLE OF CONTENTS

CHAPTER I

INTRODUCTION

1.1 Introduction to Nondestructive Testing

Advance technology provides convenience in many aspects of modern life. A jet plane enables a journey from Spain to Jamaica in less than 15 hours, much shorter than that of Christopher Columbus back in 1942. The Great Seto Bridge spans more than 13 kilometers connecting Honshu and Shikoku islands, whose existence is vital. Subway transportation systems are crucial in many big cities in the world. The increasing numbers of people combined with less available land causes buildings to grow vertically instead of horizontally; skyscrapers are becoming a common sight everywhere. These are just a few examples of the impact technology has today. Many people are extensively using these public facilities each and every day; therefore, their structural integrities must be guaranteed for their safety. The recent incident of a commercial building's collapse in Bangladesh, causing fatalities of more than 1000 people, reminds us of the importance of structural integrity. Safety aspect should be taken into account from the beginning of the structure's design, followed by a regular inspection and maintenance. The field of nondestructive evaluation plays an important role for this inspection. For instance, nondestructive evaluation is an integral part of an airplane's inspection. All parts of an airplane, in particular, have to be carefully inspected in a regular manner. This is because they experience an extreme environmental change between the landing and flying conditions, which has a significant impact to its body parts.

Of all the industries and technologies that require regular maintenance and inspection, the energy sector is of prime importance. It works to maintain economies and our daily livelihood. Up until now, the main sources of energy have been either hydrocarbon-based or nuclear. Processing crude hydrocarbons to make ready-to-use forms of energy (oil, gas, etc.) requires a complicated refining facility. A comparable complexity also exists in power generation facilities with a nuclear reactor. Plate and pipe structures, as well as huge vessels in large quantities are integral to the design of such power plants. Inspections of these infrastructures are significantly important because dangerous materials are involved. Furthermore many power plants are aging – for example, in Japan, many of them were constructed in the 1960s. After refinement

processing, the oil and gas products need to be distributed. Pipelines are the most preferable method for transporting these chemicals. This leads to a continuously-expanding research effort of pipeline inspection techniques.

The terms nondestructive evaluation/testing/inspection (NDE/T/I) refer to the same field, which generally can be defined as an examination, test or evaluation performed on any type of object without changing or altering the shape or properties in any way [1]. According to this definition, NDT has been performed in some form or another for quite some time – for instance, by a blacksmith as well as a bell-maker who carried out an ancient “sonic” based examination. While NDT on a scientific basis was established prior to the 1920s, the most significant progress of NDT was made by the tremendous activities during the Second World War.

In addition to the infrastructures, NDT is also important and applicable throughout process in industry to ensure the quality of products. NDT was once an empirical technology based on the use of off-the-shelf equipment that produced data for correlation with benchmark results by the subjective judgment of operators [2]. This empirical technology successfully met the needs of NDT for decades when the requirements were not too demanding. However, as requirements increased, mainly driven by the demand for cost reductions in life-cycle management of structures, a quantitative approach soon emerged. Quantitative NDT encompasses multiple engineering disciplines, including quantitative measurement techniques, modeling, statistics, flaw detection and characterization, and so on. There are several NDT techniques such as magnetic based testing [3], radiographic [4], ultrasonic [5], eddy current testing [6], acoustic emission testing [7] and so on. Ultrasonic based methods provide special advantages regarding its capability to probe inside the inspected material, in contrast with magnetic or eddy current testing which are only capable of surface or near-surface inspection [8].

1.2 Pipe Inspection

1.2.1 Available inspection methods

Pipeline systems are extensively used to transport various kinds of liquid and gas such as sewage, slurry, water, or even beer, but probably the most significant application is for oil and gas transportation. This is a high-risk application because it transports a highly-pressurized flammable material. Many terrible disasters as a result of pipe ruptures have occurred leading to serious economic disruptions, environmental impact, and even the loss of human life [9, 10]. One

significant cause of these accidents was corrosion, causing thinning of pipe's wall, ultimately resulting in induced rupture [11, 12]. Despite the fact that some oil and gas transportation systems are now employing polyvinyl chloride (PVC) based pipes, steel pipes are still widely being used. For that reason, any efforts to develop better methods of pipe thinning inspection are always encouraged. Moreover, it is preferable that the method is applicable for harsh environments such as high temperature or unclean areas where many pipelines are installed.

There are two broad ways to inspect the integrity of a pipe: by destructive and nondestructive methods. Common destructive methods are accomplished by means of hydrostatic inspection whose purpose is to verify that the pipe is within the predefined safety range of operation. This destructive procedure is not preferable for use during operation since it requires the pipeline system to be shut down; therefore, it is generally applied before installation of the pipe. The available nondestructive methods include magnetic flux leakage (MFL) [13-15], eddy current [16-18] and ultrasonic. Among these inspection methods, the ultrasonic method offers the ability to inspect the whole-wall thickness (not only the surface or near surface as in the case of other methods). In particular, ultrasonic NDT with guided waves [19-25] has been attractive for various reasons and will be further explained in the Chapter II.

The MFL method is applicable in a ferromagnetic material and constructed by a static magnetic field source and a Hall effect sensor. A static magnetic field flows through the inspected region. Any defect causes a change in magnetic reluctance in the closed magnetic circuit, resulting in a change in the amount of flux 'leaked' into air, which is detected by the Hall sensor. In eddy current testing, a coil which is connected to an AC source will generate a magnetic field. In the vicinity of a conductive material, eddy current will be induced in the surface of the material. This eddy current in turn will generate a second magnetic field. The presence of a defect will alter the eddy current and the induced magnetic field, which can be detected by another coil. Figure 1.1 illustrates the work principles of the two methods.

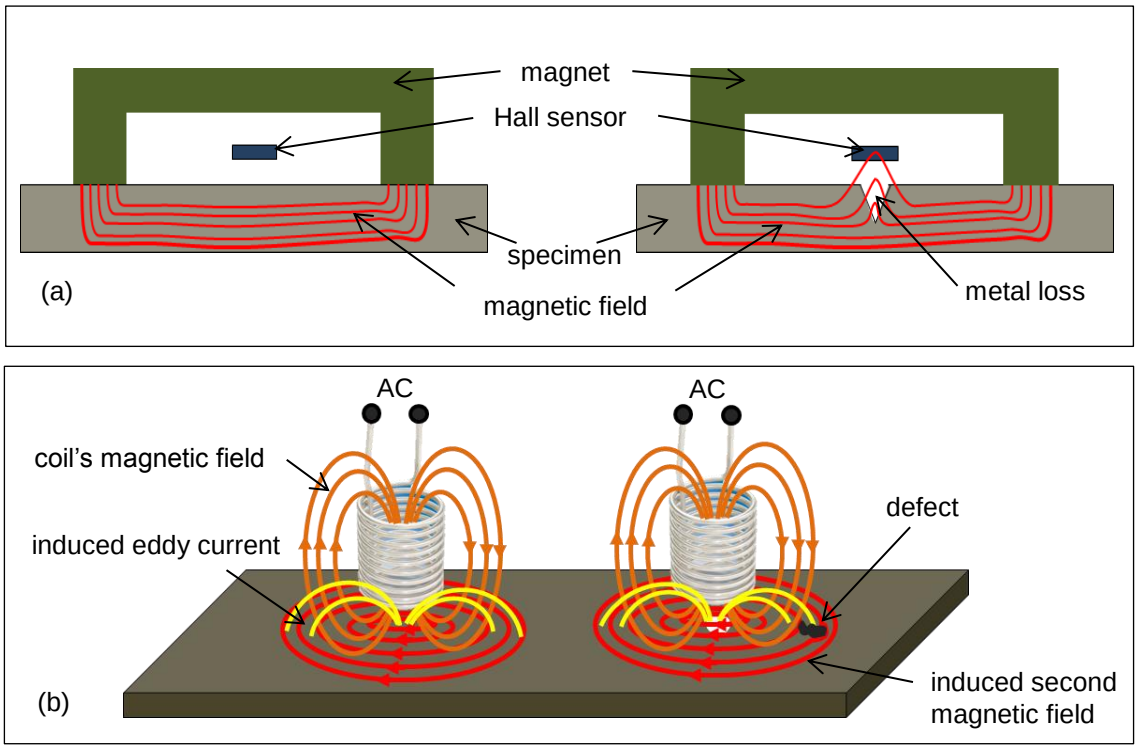

Figure 1.1 Basic principles of a magnetic flux leakage (a) and an eddy current inspection method (b).

1.2.2 Ultrasonic NDT for pipe inspection

Ultrasonic NDT remains as a workhorse of nondestructive inspection. It is realized either by a contact measurement or in a noncontact manner. Contact measurement uses a piezoelectric based transducer to generate and detect the propagating acoustic wave. The wave is generated inside the transducer and a couplant material is required to establish intimate contact with the specimen in order to enable the transmission of the wave into the specimen. This need for a couplant creates some problems. One such issue is the unreliability of the received signal because it contains information from the couplant in addition to the intended signal. Property of the couplant is also highly affected by environmental conditions and it is not practically applicable for inspection at high temperatures. Necessity of a couplant also disables the applicability for a high-speed moving inspection. With this transducer the surface of the inspected material needs to be cleaned before running the inspection, ultimately requiring a longer preparation time.

The available techniques to generate and detect acoustic waves in a noncontact manner are magnetostrictive transducers [26-28], air-coupled transducers [29, 30], laser-based ultrasonic

[31, 32] and electromagnetic acoustic transducers (EMATs) [8, 33]. These noncontact methods are of increasing interest due to the benefits of being noncontact in nature and eliminating the necessity of problematic couplant materials. EMATs are applicable to any conductive and magnetic material, while magnetrostrictive transducers are only applicable to inspect ferromagnetic materials. The configuration of a magnetostrictive transducer requires a mechanical bonding of a magnetoctriction metal atop the specimen; therefore it is not an entirely non-contact transducer. Large differences in mechanical impedance between air and the inspected material result in a relatively low efficiency of air-coupled transducers. Laser-based ultrasonic systems combine the ultrasonic generation by laser illumination and the detection by interferometric technique. J.L. Rose *et al.*, reported a laser based guided waves experiment for tubing [34]. Laser system is typically bulky and expensive. EMATs can generate an individual guided mode, depending on the driving frequency, in contrast with laser-based ultrasonic, which excites all possible modes of elastic wave [35]. In addition, EMATs can easily generate and detect torsional waves – something not possible for air-coupled transducers.

The common method of inspection with ultrasonic is based on the amplitude difference of a reflected signal from a defect. This method relies on the signal strength which is highly vulnerable to many factors such as contacting condition and background noise. For generation with EMAT, it is also affected by the magnet/current intensities and lift-off from the specimen surface.

1.2.3 Defect detection methodologies

In general, there are two methodologies of defect detection and characterization: pulse-echo and pitch-catch methods. With the pulse-echo method, evaluation of a defect or any discontinuity is based on a reflected echo signal from the defect. It usually uses the same transducer for generation and detection. While in the pitch-catch method, the waves are excited by a transmitter and propagated through the defective area. The propagating waves are detected by a receiver and the defect evaluation is based on this through-transmission signal. Figure 1.2 illustrates the both methods, notice that the transducer works as transmitter and receiver in the pulse-echo method.

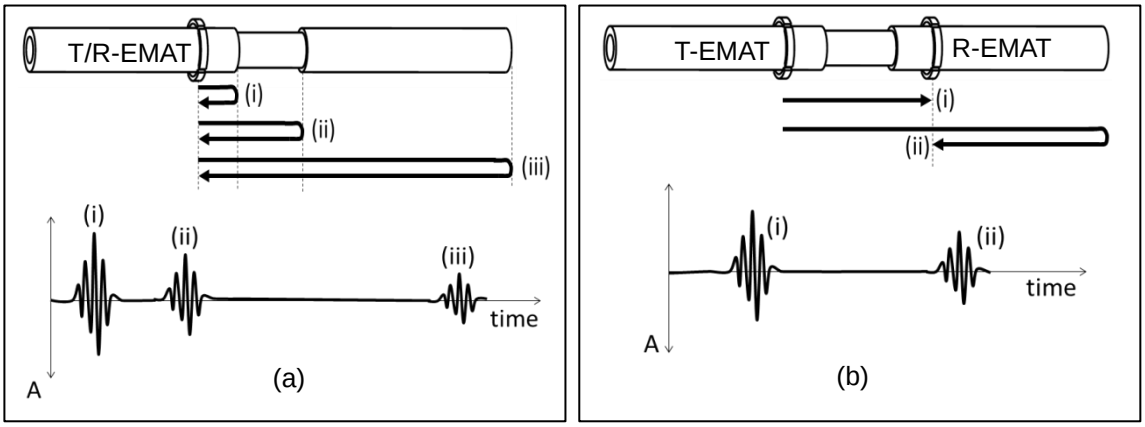

Figure 1.2 Pulse-echo (a) and pitch-catch (b) inspection methods.

1.3 Proposed Inspection Method

There are two main issues with ultrasonic method for pipe inspection, as previously mentioned:

1. The necessity of intimate contact between the transducer and the specimen which limits the condition and speed of the inspection.
2. The susceptibility of signal strength of amplitude based method on many factors described earlier.

The present study attempts to address the two issues simultaneously by proposing a novel ultrasonic method for pipe inspection. The non-contact type transducer, EMAT, is used to generate and detect the ultrasonic waves, hence solving the first problem. A new approach of inspection based on a change in group velocity is proposed as an alternative to the amplitude based method.

Torsional guided wave is particularly chosen as a tool of inspection based on the proposed method for several reasons. Among guided waves, this wave offers more benefits because the component of particle displacement is only in the circumferential direction. This feature makes torsional modes insensitive to liquid loading and insulation material, which often covers a pipe in many applications. The modes consequently propagate over a longer distance. More importantly, this wave has a simple dispersion characteristic leading to an easier interpretation. Figure 1.3 compares the group velocity dispersion curves of torsional and Lamb guided waves, where the simplicity of torsional wave is apparently seen.

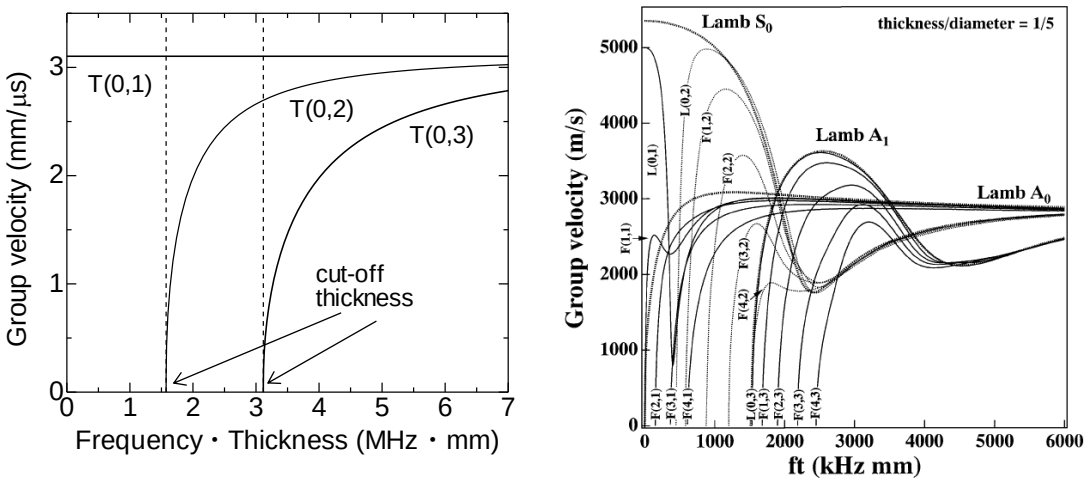

(a) (b)

Figure 1.3 Group velocity dispersion curves of the torsional (a) and the Lamb modes [39] (b).

Taking advantage of this simple dispersion behavior, the present study proposes a novel method for pipe inspection based on a group velocity change of the torsional waves induced by mode conversion. Except for the fundamental T(0,1) mode, torsional guided wave is dispersive, which means the velocity depends not only on the material but also on thickness×frequency, as shown in Fig. 1.3(a). Furthermore, there is a specific thickness for each higher mode, the so called "*cut-off thickness*", below which that mode cannot exist. At this thickness, vibrational mode of the associated mode cannot be supported; it is then expected to convert to lower mode(s) with a higher group velocity in order to continue propagating. By keeping the frequency fixed, the group velocity becomes dependent solely on the thickness, providing a basis for wall-thinning inspection. This method has been successfully applied by the author to the case of a shear horizontal (SH) guided waves propagating in a plate specimen [36-38]. This study is then carried out to extend the method to the measurement of torsional waves in a pipe. However, generating a pure torsional waves is a lot more challenging than that of the SH guided waves.

1.4 Outline of the Thesis

My study was motivated by the importance of wall-thinning detection and characterization, especially in pipe structures. In the effort to contribute to that field, a new and novel inspection method combining the reliable method based on traveling time measurement and the superiority of a non-contact measurement technique is proposed. This thesis will report the extensive works that have been performed and the experimental results to support the proposed method.

The proposed method takes advantage of the dispersive characteristic of the torsional guided waves. Therefore a deep understanding on this matter is required. Chapter II presents an introduction to the torsional waves and its excitation. The section on torsional guided waves is started by highlighting the advantages of guided waves as an inspection tool. The dispersion relations, along with some important parameters, are introduced. Several available methods to generate torsional waves will be mentioned. This will segue to a description of the electromagnetic acoustic transducer (EMAT) – identifying it as a superior generation method amongst its transducer counterparts. Summary on the basic principle of generation and detection mechanisms with an EMAT is given. The EMATs presented here are of an original design and developed in-house to suit the present study. The ability of the newly developed EMATs to generate and detect the intended modes of torsional wave is then confirmed via experimental study.

Chapter III addresses some fundamental studies to elaborate on the mode conversion phenomena. The dependence of group velocity on thickness is investigated by measuring the traveling time of torsional waves in several pipe specimens containing thinning regions. As a result of thickness changes, it is found that the observed traveling time of the higher mode decreases – a result indicating mode conversion. Based on this finding, further experimentation is performed to investigate the detailed mechanism of this conversion. The influence of defect shape on mode conversion is also examined, which leads to an intriguing discovery of a total reflection of higher modes.

Chapter IV covers some applications of the proposed method to inspect a variety of pipe defects. Partial-circumferential defects are successfully detected by the proposed method, indicating that the mode conversion occurs even when the thinning region does not exist around the entire circumference. The minimum axial length of a fully-circumference defect which induces mode conversion is also investigated. It is found that the conversion occurs when the length is comparable or more than the generated wavelength. A system of two identical EMATs connected by a fixed-spacer is developed to permit internal inspection of pipe structures, *i.e.* the inspection is performed from within the pipe. With this system, it is possible to inspect a pipe while it is being used, eliminating the necessity to suspend the operation. This newly developed system is then used to inspect pipes containing dish-shaped defects, a commonly found form of wall thinning. The proposed method successfully detects dish-shaped defects with comparable cross-sectional losses of approximately 22% or more. An experiment to simulate the real application of the system is performed. It is used to inspect a pipe containing multiple dish-shaped defects by

moving it within the pipe while continuously measuring the relative phase and amplitude along the axial direction. The presence of a defect is clearly observed from the shift of both phase and amplitude. The measured values vary proportionally at each defect-feature. These results may potentially be able to identify different sizes of defect. Experimentations reported in this chapter show the good potential of the proposed mode conversion method for pipe inspection.

Chapter V summarizes and concludes the study. Some suggestions for actual applications are also given.

CHAPTER II

TORSIONAL GUIDED WAVES GENERATED BY EMAT

2.1 Torsional Guided Waves

2.1.1 Guided waves inspection

Inspection with guided waves has been practically implemented throughout the last few decades. Guided wave is a type of wave whose propagation is confined to and guided by the one or two-dimensional medium (waveguide), such as tubing, piping, rod, or any plate structures. Therefore, this wave can propagate longer with less attenuation, enabling the inspection of a wide area in a short amount of time. The wave propagates following the structure, enabling the user to inspect hidden areas not accessible with conventional ultrasonic testing (UT). This method of inspection is especially popular for rapid screening of a large area for the purpose of detecting the presence of any anomalous condition within the waveguide. The procedure is often followed by an additional UT inspection at suspicious locations recognized by the guided waves method for a more detailed inspection. Figure 2.1 compares the principles of both methods of inspection. Guided waves propagation is much more complicated than that of the bulk waves. It involves multi-modes with different propagation behavior. Understanding their behavior is indispensable for the optimum implementation of guided waves inspection.

Among guided waves, the torsional wave offers more benefits than others because the component of particle displacement is only in the circumferential direction. This feature makes torsional modes insensitive to liquid loading and insulation material which often covers a pipe in many applications. The modes consequently propagate over a longer distance. Furthermore, this wave has a simple dispersion characteristic leading to an easier interpretation. Many studies on this wave have been carried out. The finite element method was used to predict the reflection of the fundamental torsional mode from various defects [40-42]. Some studies on scattering were also reported [43-45]. However, most reported studies were mainly based on analytical and numerical approaches. This is because the torsional wave is not as easy to generate as the other guided waves, although a piezoelectric array [46, 47] and a magnetostrictive transducer [26-28] were used. In the present study, we use an electromagnetic acoustic transducer (EMAT).

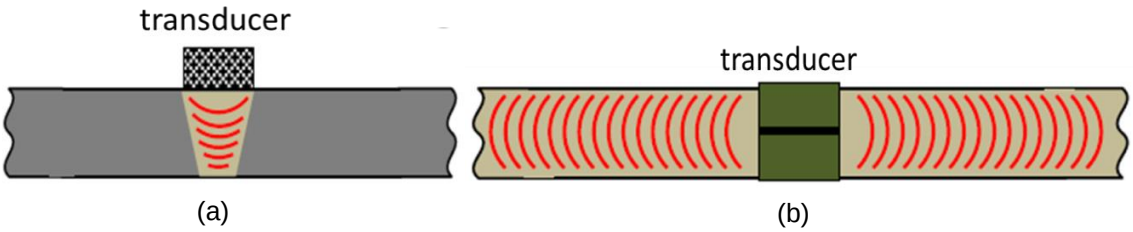

Figure 2.1 Illustration of a conventional ultrasonic testing (a) and a guided waves inspection (b). The inspected regions are indicated in light brown color with the traveling acoustic in red lines.

2.1.2 Dispersion relation of torsional guided waves [48-50].

Considering the coordinate reference in a cylindrical waveguide shown in Fig. 2.2(a), wave motion in the family of torsional waves involves only a single displacement component in θ direction, u_θ, being similar to a shear horizontal (SH) guided wave in a plate. As a convention, mode naming is defined as T(*n*,*m*), where *n* and *m* are the circumferential and radial (thickness) mode indices, respectively. Most researchers define the circumferential parameter for longitudinal and torsional waves as 0 and when *n* equals 1 or more the wave is categorized as a flexural mode. The present study adopts this convention. Particle displacement is only a function of radius while the wave propagates in the axial direction, as shown in Fig. 2.2(b). Figure 2.3 shows the particle displacement of the fundamental T(0,1) and the first higher T(0,2) modes in the cross sections of a pipe with green and red arrows indicate the direction of particle displacements.

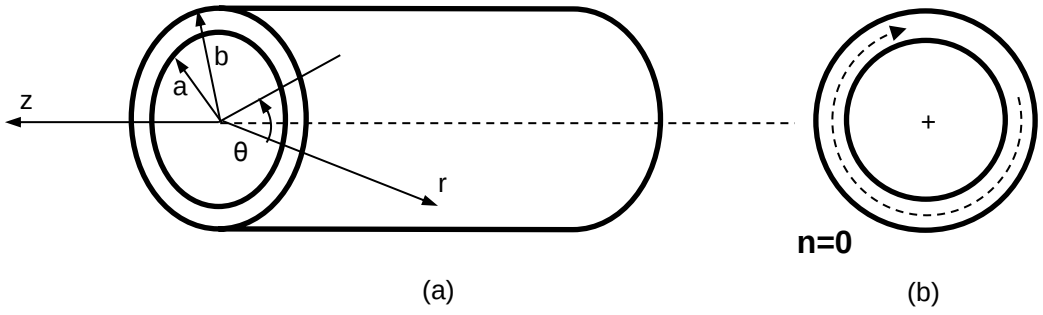

Figure 2.2 Coordinate reference (a) and circumferential vibration mode for torsional wave (b).

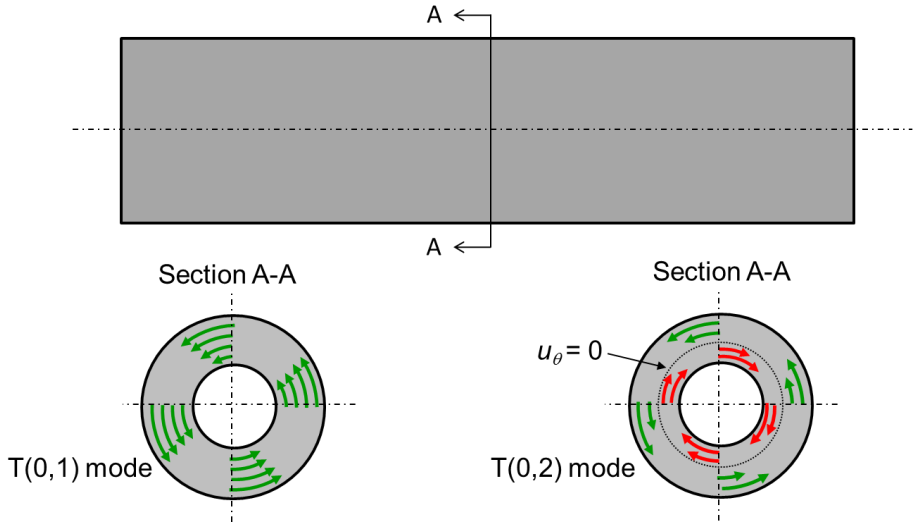

Figure 2.3 Pipe cross section showing particle displacements for the fundamental T(0,1) and the first higher T(0,2) modes. Green and red arrows indicate vibration directions.

As previously mentioned, torsional waves involve only single a displacement u_θ. By taking cylindrical coordinate as shown in Fig. 2.2, the remaining equation of motion can be written as:

$$\frac{\rho}{\mu}\frac{\partial^2 u_\theta}{\partial t^2} = \frac{\partial^2 u_\theta}{\partial z^2} - \frac{u_\theta}{r^2} + \frac{1}{r}\frac{\partial u_\theta}{\partial r} + \frac{\partial^2 u_\theta}{\partial r^2}. \tag{1}$$

Considering the propagation of sinusoidal waves along the axis, the involved displacement is

$$u_\theta = V \exp\left[i(\gamma z + \omega t)\right] \tag{2}$$

Applying this to Eq. (1) will result in

$$\frac{\partial^2 V}{\partial r^2} + \frac{1}{r}\frac{\partial V}{\partial r} + \left(\frac{\rho\omega^2}{\mu} - \gamma^2 - \frac{1}{r^2}\right)V = 0 \cdot \tag{3}$$

Assigning κ as:

$$\kappa = \sqrt{\frac{\rho\omega^2}{\mu} - \gamma^2} \tag{4}$$

Assigning $S = \kappa r$ we will have:

$$S^2\frac{\partial^2 V}{\partial S^2} + S\frac{\partial V}{\partial S} + V\left[S^2 - 1\right] = 0 \cdot \tag{5}$$

This is a Bessel equation of order one whose solution is shown in Eq. (6), where *J* and *Y* are Bessel functions of first and second kinds, respectively, while A_1 and A_2 are constants.

$$V = A_1 J_1(S) + A_2 Y_1(S) \tag{6}$$

The three stress components $\sigma_{rr}, \sigma_{r\theta}, \sigma_{rz}$ will vanish at the inner and outer surfaces of the cylinder, $r = a, b$ of Fig. 2.2. Here only $\sigma_{r\theta}$ to be considered, as the other two are zero automatically.

$$\sigma_{r\theta} = \mu\left[\frac{1}{r}\frac{\partial u_r}{\partial \theta} + r\frac{\partial}{\partial r}\left(\frac{u_\theta}{r}\right)\right] = 0 \cdot \tag{7}$$

For torsional waves, $u_r = 0$, therefore considering Eqs. (2), (6) and (7), we have:

$$A_1\left[\frac{\partial J_1(S)}{\partial S} - \frac{\partial J_1(S)}{S}\right]_{S=\kappa a} + A_2\left[\frac{\partial Y_1(S)}{\partial S} - \frac{\partial Y_1(S)}{S}\right]_{S=\kappa a} = 0 \tag{8.1}$$

$$A_1\left[\frac{\partial J_1(S)}{\partial S} - \frac{\partial J_1(S)}{S}\right]_{S=\kappa b} + A_2\left[\frac{\partial Y_1(S)}{\partial S} - \frac{\partial Y_1(S)}{S}\right]_{S=\kappa b} = 0 \tag{8.2}$$

.

Applying the recurrence relation of Bessel functions:

$$J_n(S) = \frac{1}{2}\left[J_{n-1}(S) - J_{n+1}(S)\right] \rightarrow J_1(S) = \frac{1}{2}\left[J_0(S) - J_2(S)\right] \tag{9.1}$$

$$Y_n(S) = \frac{1}{2}\left[Y_{n-1}(S) - Y_{n+1}(S)\right] \rightarrow Y_1(S) = \frac{1}{2}\left[Y_0(S) - Y_2(S)\right] \tag{9.2}$$

The dispersion relation can be represented as:

$$\begin{aligned}&\left[\left(\frac{1}{2}\left[J_0(\kappa a) - J_2(\kappa a)\right]\right) - \frac{J_1(\kappa a)}{\kappa a}\right] \cdot \left[\left(\frac{1}{2}\left[Y_0(\kappa b) - Y_2(\kappa b)\right]\right) - \frac{Y_1(\kappa b)}{\kappa b}\right] - \\ &\left[\left(\frac{1}{2}\left[Y_0(\kappa a) - Y_2(\kappa a)\right]\right) - \frac{Y_1(\kappa a)}{\kappa a}\right] \cdot \left[\left(\frac{1}{2}\left[J_0(\kappa b) - J_2(\kappa b)\right]\right) - \frac{J_1(\kappa b)}{\kappa b}\right] = 0.\end{aligned} \tag{10}$$

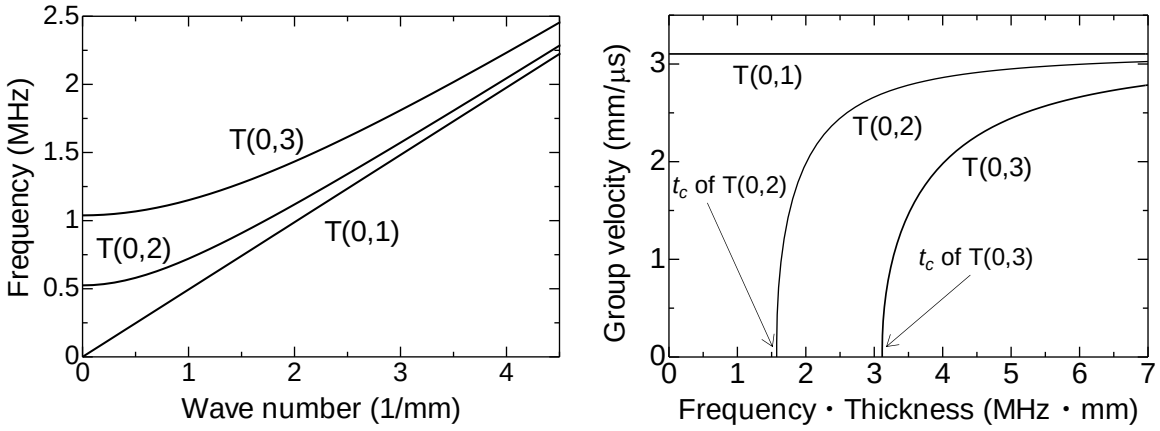

(a) (b)

Figure 2.4 Dispersion curves of torsional wave propagation in an aluminum pipe with inner/outer diameters of 19/25 mm, for wavenumber-frequency relation (a), and frequency × thickness-group velocity relation (b).

Figure 2.4(a) shows the dispersion curves up to the second higher T(0,3) mode. They are derived numerically from Eq. (10) for an aluminum pipe (ρ=2.7x10^3 kg/m^3, μ=26 GPa) with inner and outer radii of 9.5 and 12.5 mm, respectively. This is one of the specimens used in the present study. Group velocity is defined as $c_g = d\omega/d\gamma$ and its corresponding dispersion curves are also presented in Fig. 2.4(b). The fundamental T(0,1) mode is non-dispersive and its group velocity is constant. However, those of higher modes depend on the frequency×thickness and the dependencies are even more pronounced in the lower frequency range. There is a critical point for every higher mode where the group velocity is zero. When the operating frequency is maintained at a fix value, this point corresponds to the so-called cut-off thickness, t_c. This is an important term firstly introduced in the present study.

2.2 Electromagnetic Acoustic Transducer

2.2.1 Introduction

The common transducer used for acoustic wave generation takes advantage of the piezoelectric (and reverse piezoelectric) effect [51]. With the piezoelectric effect, a mechanical vibration will be generated in the piezoelectric element when the crystal is driven by an electric field. The opposite phenomenon occurs with the reverse piezoelectric effect. Thus, the elastic wave is generated in the transducer itself. For actual application, this generated wave needs to be transmitted into the inspected specimen where the wave is propagated. An intimate contact between the transducer and the specimen is necessary. This is usually accomplished by using a couplant material, illustrated in Fig. 2.5(a).

An EMAT has the ability to convert electromagnetic energy into mechanic energy and vice versa. It works with a totally different mechanism than the piezoelectric transducer. The electromagnetic acoustic transduction occurs across an air gap, eliminating the need for an intimate contact between the transducer and the inspected material. EMATs are completely noncontact transducers; therefore, those disadvantages associated by the couplant usage do not exist. EMAT is well recognized for its ability to generate some wave types that are difficult with a piezoelectric transducer. Such examples are the SH guided wave in a plate and torsional wave in a pipe. An alternative to the EMAT for generating these waves is the magnetostrictive transducer [26-28]. However, the configuration of this transducer requires the mechanical bonding between a material which has a high magnetostriction (typically nickel) and the specimen. This transducer is still a contact-type transducer. Figure 2.5(b) shows a typical configuration of this transducer. Being different from a laser-based system, which generates all possible types of waves, an EMAT has the ability to selectively generate and detect a specific, intended mode of waves. When inspecting with guided waves, the complexity of waves is often unavoidable. The selectivity feature of EMAT is then important in order to focus only on the intended mode of waves.

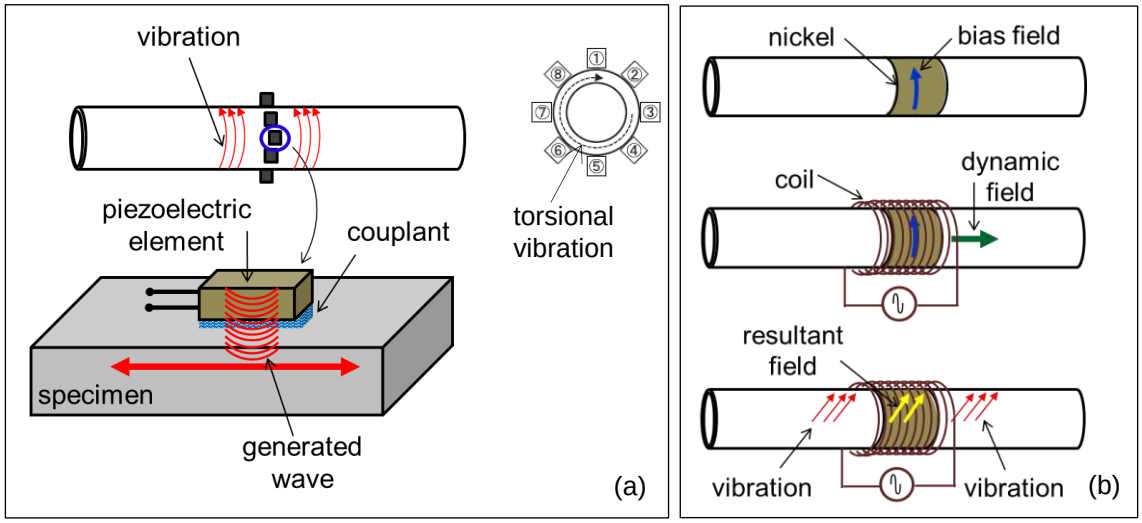

Figure 2.5 Torsional wave generation with an array piezoelectric transducer (a) and a magnetostrictive transducer (b).

2.2.2 Generation and detection mechanisms

There are three mechanisms responsible for electromagnetic-acoustic coupling: the Lorentz force, magnetostriction and the magnetization mechanisms. Magnetostriction is a property of materials that causes a change of their dimensions during the process of magnetization. The Lorentz force mechanism applies in any conductive material. In a ferromagnetic material, all mechanisms take place in the transduction process. Extensive studies have been performed to identify which mechanism dominates the transduction [52, 53]. According to the latest study, the Lorentz force is the main method of transduction in a non-oxidized ferromagnetic material. An EMAT is constructed with a permanent magnet or an electromagnet as a source for a biased static magnetic field, **B**, and a coil. When an alternating current is applied to this coil, which is placed adjacent to a conductive material, an eddy current with density **J** is induced within the skin depth of surface layer of the material (for aluminum, 8.46 μm at a frequency of 1 MHz). By way of the Lorentz force mechanism, interaction between **J** and **B** induces deflection of the material's electrons, resulting in a body force. Here, $\mathbf{F}_L$ is known as a Lorentz force per unit volume. The resultant body force generates elastic waves whose type and direction depend on the relative direction between the biased magnetic field and the induced eddy current (the cross product of Eq. (11)).

$$\mathbf{F}_L = \mathbf{J} \times \mathbf{B} \tag{11}$$

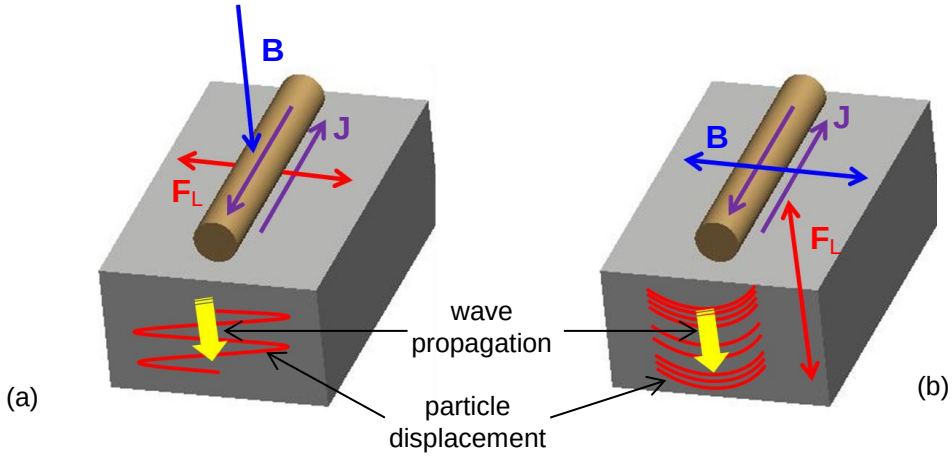

Figure 2.6 Generation of shear (a) and longitudinal (b) vibration with EMAT.

Figure 2.6 shows a schematic representation of shear and longitudinal waves propagating in the thickness direction. The reverse Lorentz force mechanism occurs at the receiving side. An acoustic wave induces a dynamic deformation in the material. In a conductive material exposed to a static magnetic field, this dynamic deformation creates dynamic magnetic fields. The receiving coil detects these dynamic magnetic fields after the signal traverses the boundary between material and air. The air gap between the material and the coil (the *lift-off)* exponentially decreases the transduction efficiency. Detailed explanation of the transduction theory can be found in many references [8, 33, 52-53].

2.2.3 Arrayed periodic permanent magnet (PPM-EMAT)

In the present study, handmade EMATs with an original configuration are developed. The design is based on the so-called periodic permanent magnet (PPM) EMAT. Previous work utilized a basic PPM-EMAT configuration [8, 35, 54]. In a PPM-EMAT, dynamic and static fields are generated by an elongated spiral coil and permanent magnets, respectively. The permanent magnets lie atop of the coil such that direction of the static magnetic field is perpendicular to that of the dynamic fields. The permanent magnets are arranged in such a way to accommodate a periodically alternating magnetization perpendicular to the specimen's surface. In the PPM-EMAT, the periodicity of magnet arrangement in the axial direction determines the wavelength of the wave to be generated. The present EMAT generates torsional waves with a fixed wavelength of 5.22 mm. Figure 2.7 shows the configuration of a PPM-EMAT to generate a shear horizontal vibration in a flat surface and mechanism of the Lorentz force generation.

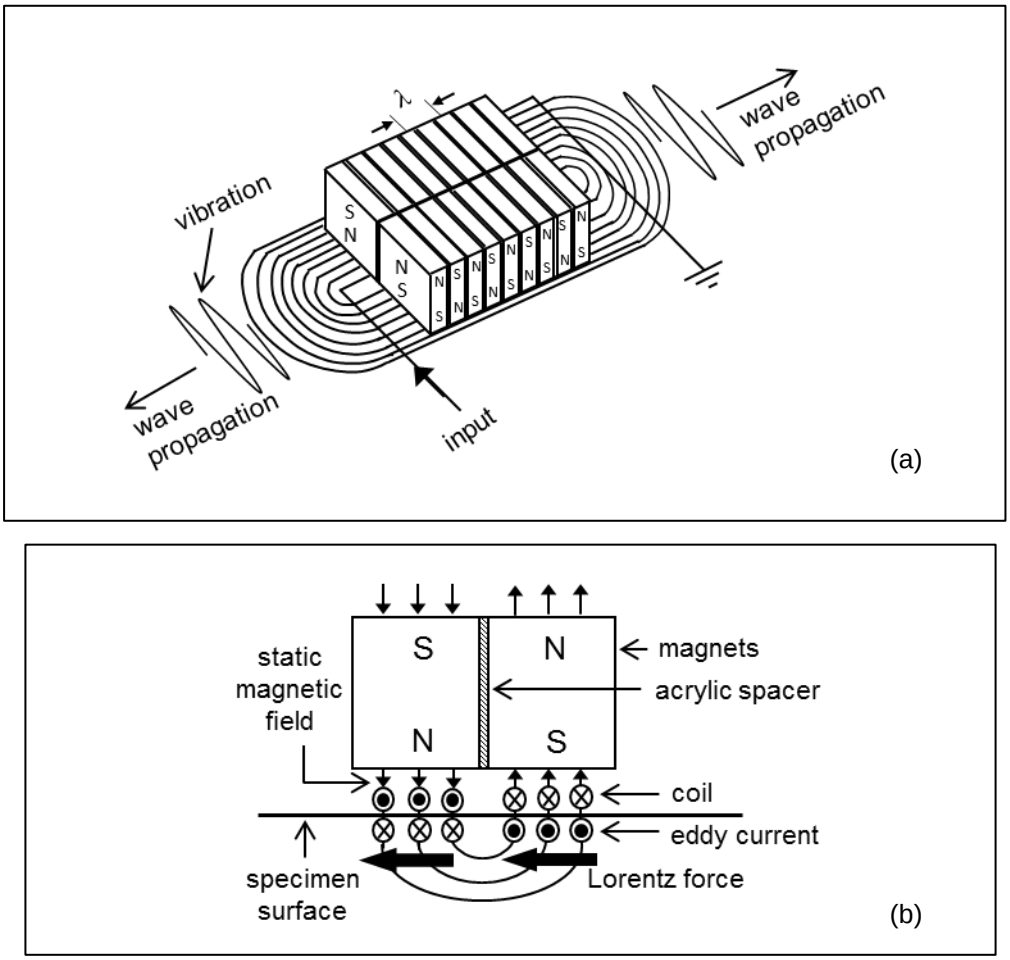

Figure 2.7 A PPM-EMAT for generation a shear horizontal vibration in a plate (a) and the mechanism of a Lorentz force generation (b).

In the present EMAT for generating torsional waves in a pipe, four PPM-EMATs were arranged to form a meandering pattern and placed around the pipe specimen. One EMAT consists of a wound coil and two pairs of magnet arrangements with opposite magnetizations. One set of magnet arrangements provides a static magnetic field to two neighboring coils. There are seven magnets in each arrangement such that the total number of magnets is twenty eight. They are Neomax Nd-Fe-B magnet, 10 mm in height and 2.5 mm thick. Enameled copper wire with a diameter of 0.2 mm is used to build the coil. Figure 2.8 shows the placement of the four PPM-EMATs on a pipe specimen, the cross sectional view of their arrangement, and the involved fields in the transduction process. The excited waves propagate along the axial direction of the pipe. Lift-off between the EMAT and the specimen is approximately 0.11 mm.

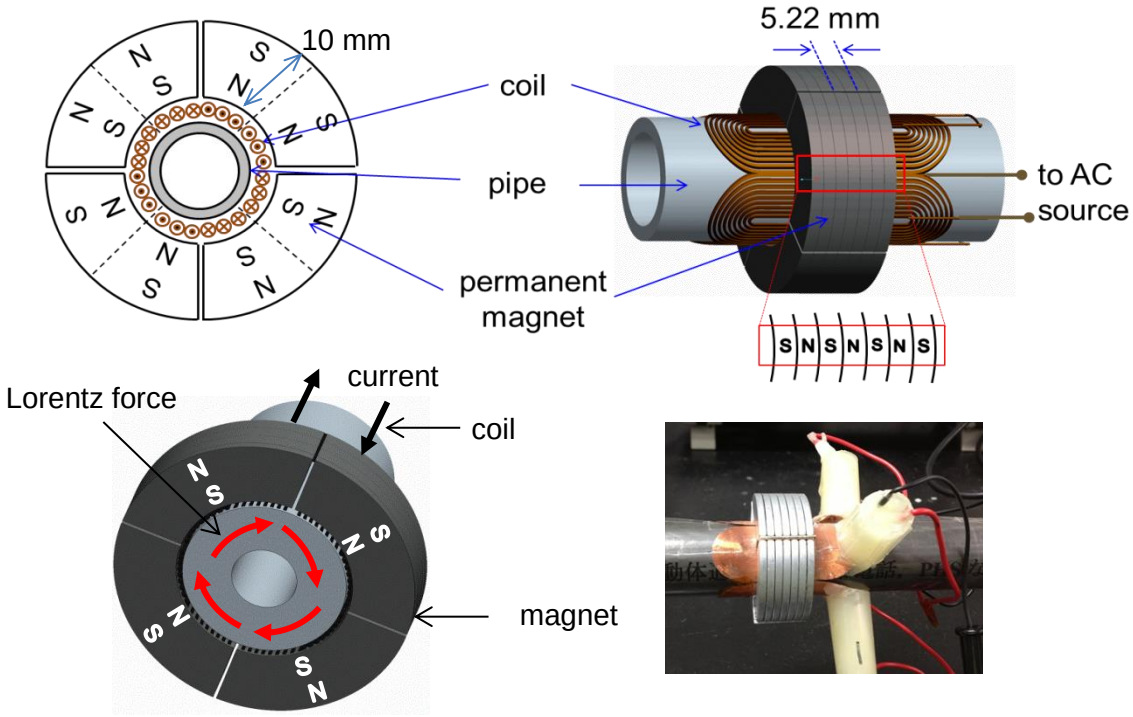

Figure 2.8 EMAT's placement around the pipe, cross-sectional view of EMAT's arrangement, and the Lorentz force generation. Dashed lines separate each PPM-EMAT. Picture of an actual EMAT is also presented.

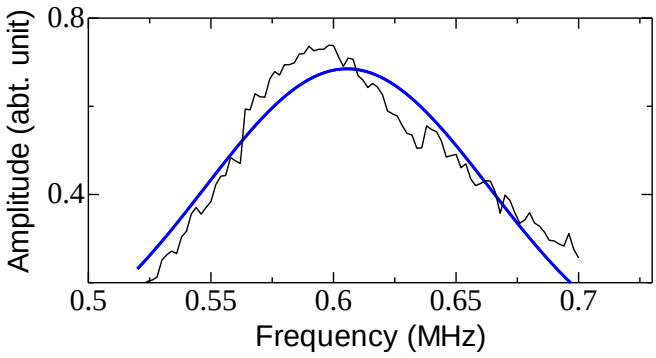

Figure 2.9 Frequency responses from which the operating frequency of 0.615 MHz is determined by performing a Gaussian fitting (shown in blue line).

2.3 Torsional waves generation with arrayed PPM-EMAT

Aluminum pipes are used as specimens in the beginning of the present study for fundamental investigations. This material is chosen because it is relatively easy to generate elastic waves and to fabricate defects within it. However, steel pipe is more widely used in practical application and further study is then performed with steel pipes. The optimum operating frequency for each torsional mode is obtained by sweeping the amplitude over a range of frequencies around the theoretical value determined from the dispersion equation. A Gaussian fitting is applied to the frequency response in order to find the frequency which gives the optimum response. Figure 2.9 shows the typical frequency response for frequency of 0.52-0.7 MHz, from which the optimum frequency of 0.615 MHz is obtained. The blue line shows the Gaussian fitting.

2.3.1 Aluminum pipe

The fundamental T(0,1), the first higher T(0,2) and the second higher T(0,3) of torsional modes can be excited in aluminum pipes by the above described EMAT. The aluminum pipe is 1000 mm long with thickness and outer diameters of 3 and 25 mm, respectively. The optimum frequencies are 0.615, 0.77 and 1.18 MHz, for the generation of the T(0,1), T(0,2) and T(0,3) modes, respectively. Figure 2.10 shows a comparison of these values against the theoretical dispersion curves. Group velocity is determined by gating out the intended signal and measuring the phase-shift dependence of the frequency. More detail explanation about this procedure will be presented in Chapter III. The observed group velocities are 3.12, 2.22 and 1.53 mm/μs for the T(0,1), T(0,2) and T(0,3) modes, respectively. Figure 2.11 shows the waveform of each mode and its experimental group velocity plotted against the calculated dispersion curves. Figures 2.10 and 2.11(d) show a good agreement between the parameters obtained by experiment and theory. From this it can be shown that the generated modes are indeed the T(0,1), T(0,2) and T(0,3) modes.

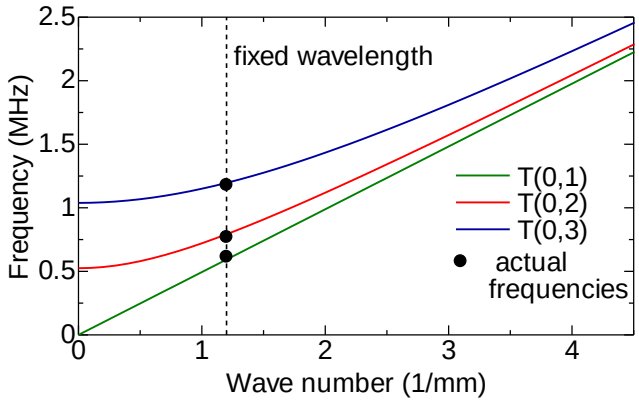

Figure 2.10 Actual operating frequencies plotted against the theoretical dispersion curves.

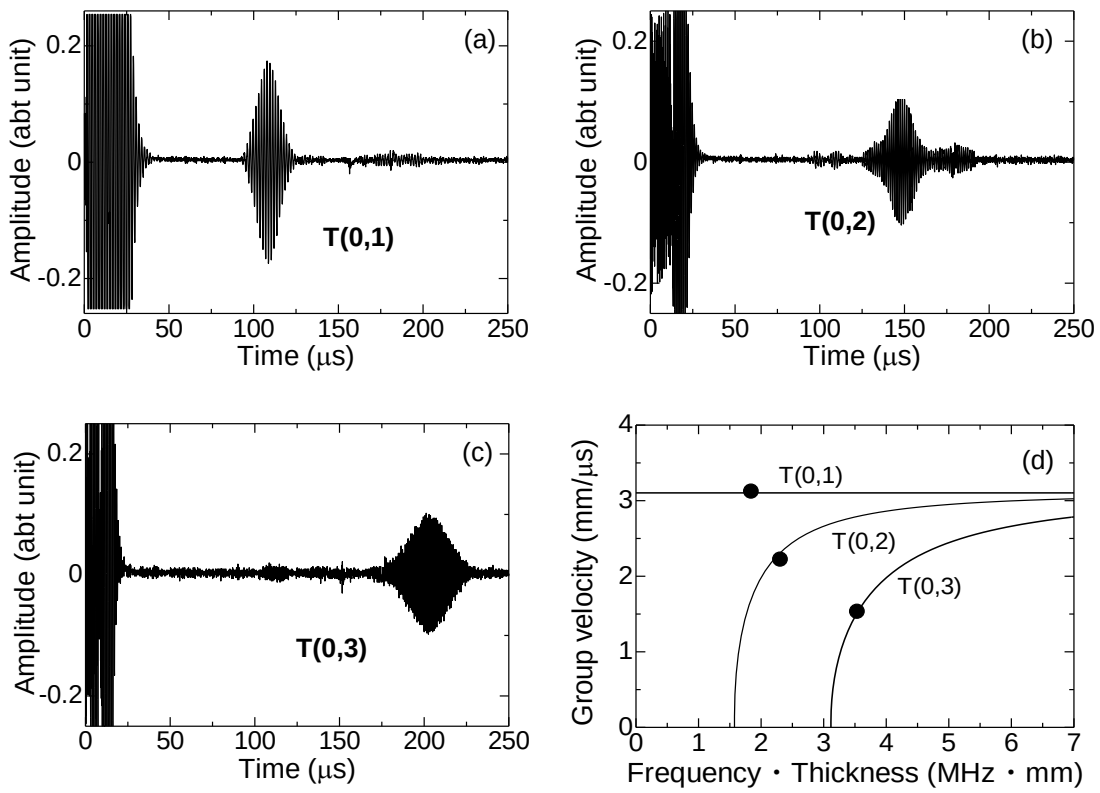

Figure 2.11 Typical waveforms of (a) T(0,1), (b) T(0,2) and (c) T(0,3) modes propagated in an original defect-free pipe. Experimental group velocities of each mode are plotted against the calculated group velocity dispersion curves (d).

The torsional waves can propagate over long distances with less attenuation, as previously mentioned. A pair of transmitter and receiver EMATs separated by 450 mm are used to generate and detect a T(0,1) mode in a 1500-mm long defect-free pipe. Figure 2.12 shows the placement of the EMATs around the pipe and received signals showing multiple reflections from the ends of the pipe. The direct received signal is indicated by **(i)** in the figure. Signal **(ii)** has higher amplitude as result of a constructive interference of two reflected signals propagating in the same distance from both ends of the pipe. The furthest signal shown in the figure is obtained after propagating more than 15 m.

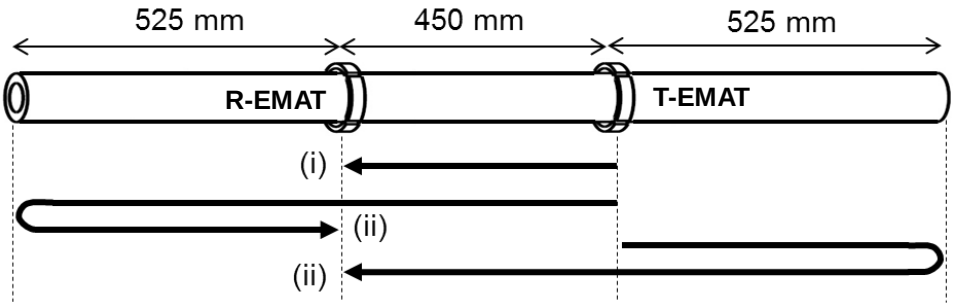

(a)

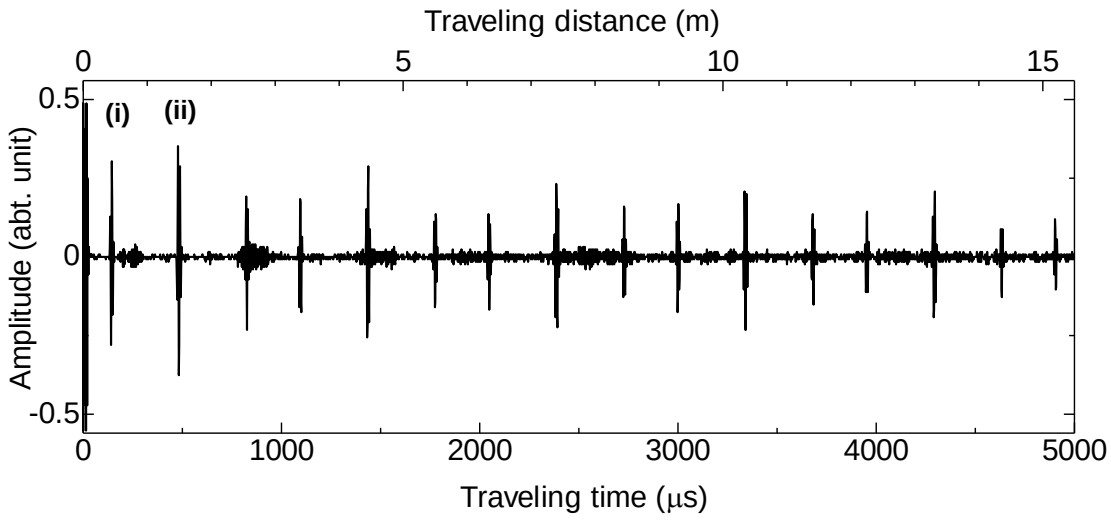

(b)

Figure 2.12 Multiple echoes of the generated waves from the ends of the pipe showing insignificant attenuation. The furthest signal corresponds to a propagation distance of more than 15 m.

2.3.2 Steel pipe

The same EMAT configuration can generate T(0,1) and T(0,2) modes in a 3.5 mm thick (outer diameter of 25.4 mm) steel pipe. They are generated at the operating frequencies of 0.6 and 0.78 MHz, respectively. The experimental group velocity of each mode is 3.22 and 2.52 mm/μs. Figure 2.13 shows typical waveform of each mode and the comparison of these values against the theoretical dispersion curves. The experimental and theoretical parameters are also found to have a good conformity, indicating that the intended T(0,1) and T(0,2) modes are generated.

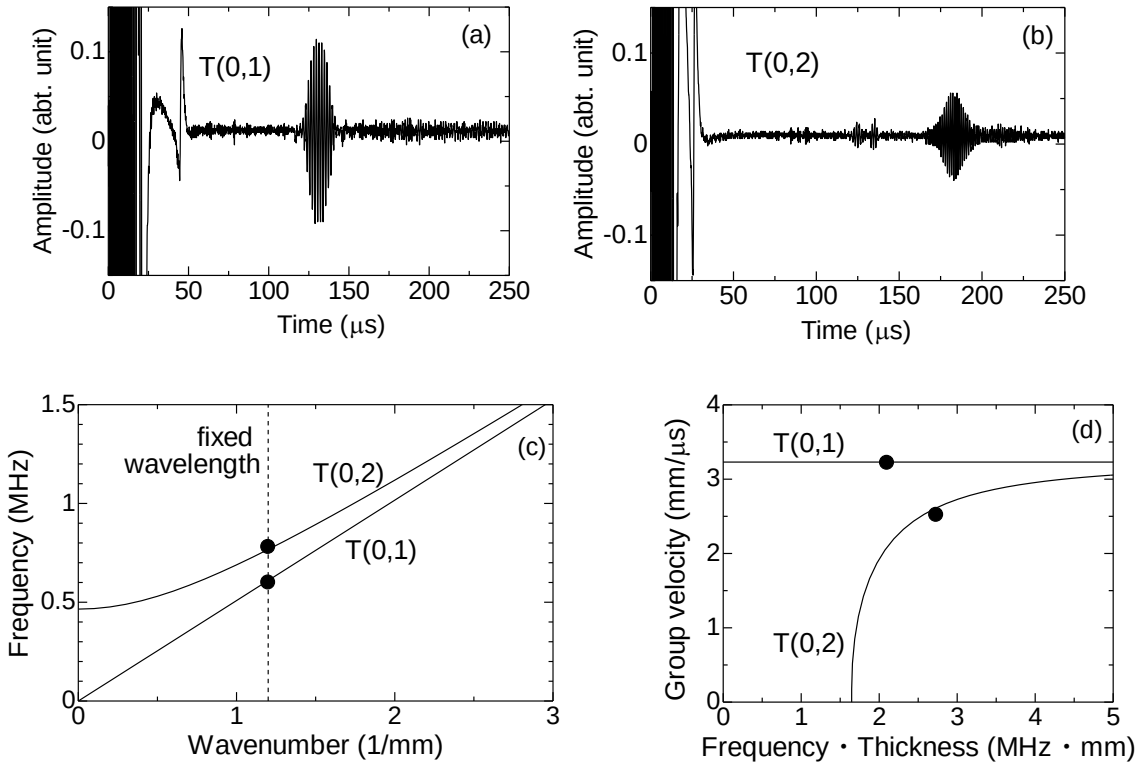

Figure 2.13 Typical waveform of the generated T(0,1) mode (a), and of the T(0,2) mode (a) in a defect-free steel pipe. Comparison between the experimental and theoretical dispersion curves of the operating frequencies (c) and group velocities (d).

2.3.3 Circumference distribution

The EMAT was designed to excite torsional waves uniformly along the circumference of the pipe. A simple investigation is performed to investigate the amplitude distribution along the circumference of the pipe. The T(0,1) and T(0,2) modes are generated by an EMAT and the propagating waves are picked up by a needle-type transducer located 400 mm away from the EMAT. The needle transducer and the pipe are fixed and the EMAT is rotated by every 22.5° such that the propagating waveforms at 16 positions along the circumference are obtained. All the measurement points are located at the same axial plane, as illustrated in Fig. 2.14. Figure 2.15 shows the received waveforms at these measurement points, for these two modes generated. The intended mode is the signal of the maximum amplitude. The fundamental T(0,1) mode is also excited (with much smaller amplitude) when the T(0,2) mode is generated, as shown in Fig. 2.15(b). For these two modes, the waves are observed in all circumferential positions with approximately the same amplitude. It indicates the uniformity of the generated waves along the circumference of the pipe.

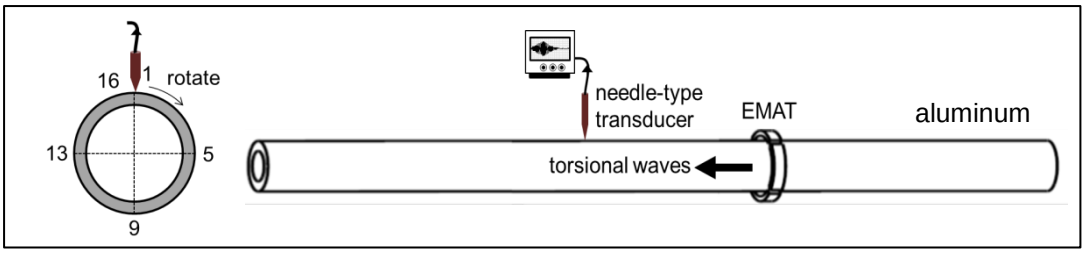

Figure 2.14 Placement of the transducers around a pipe.

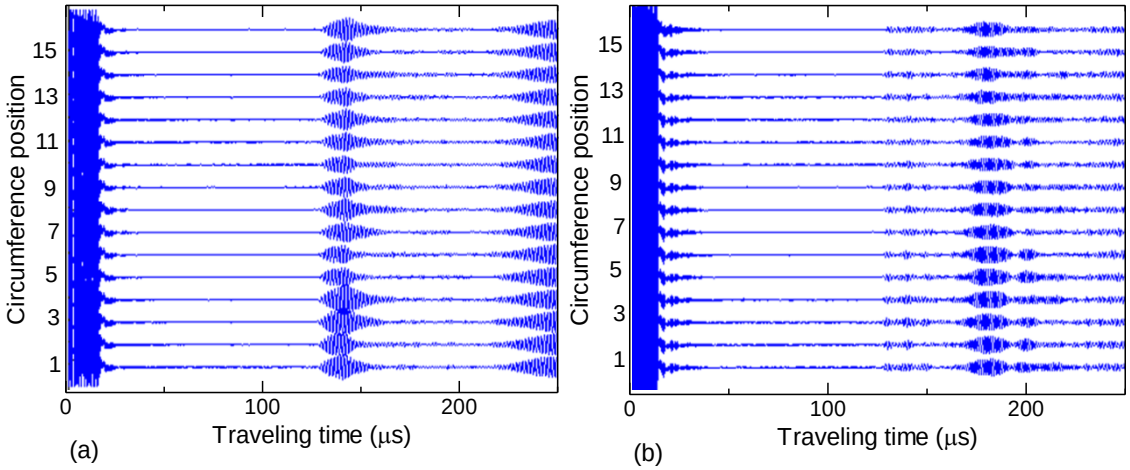

Figure 2.15 Received waveforms at each circumferential position for the T(0,1) mode (a) and T(0,2) mode (b) generated.

CHAPTER III

FUNDAMENTAL STUDIES

3.1 Introduction

The present study proposes a new method for pipe inspection based on group velocity change caused by mode conversion. Inspection with this method heavily relies on a traveling time measurement in contrast with the common amplitude based measurement. This chapter covers some fundamental studies performed to support the idea and to investigate the propagation behavior of torsional waves for a better understanding of this wave. The fundamental T(0,1) and first higher T(0,2) modes are generated in pipe specimens by an arrayed PPM-EMAT. Depending on the objective of the experiment, another EMAT or a needle-type piezoelectric transducer is used in the receiving side. The pipe specimen is mainly of A5052 aluminum alloy. This material is malleable and it is easier to fabricate a defect on it. The observed propagation behavior should be independent on the type of material. For confirmation, some experiments are repeated in pipe specimens of steel S45C because steel still remains as the most widely used material in many pipe applications. The chemical compositions of the two materials are presented in Tables 3.1 and 3.2, respectively. All of the specimens have the same total length of 1000 mm. The aluminum pipe has an outer diameter of 25 mm (3 mm thickness) and that of the steel pipe is 25.4 mm (3.5 mm thickness).

Table 3.1 Chemical composition of A5052 aluminum alloy (% weight)

% Si	% Fe	% Cu	% Mn	% Mg	% Cr	% Zn	% Al
0.25 max	0.40 max	0.10 max	0.10 max	2.2 – 2.8	0.15 – 0.35	0.10 max	bal*)

*) remaining material composition

Table 3.2 Chemical composition of S45C steel alloy (% weight)

% C	% Si	% Mn	% P	% S	% Fe
0.42 – 0.48	0.15 – 0.35	0.6 – 0.9	0.030 max	0.035 max	bal

3.2 Experimental Procedure

The typical experimental setup is presented in Fig. 3.1. The superheterodyne spectrometer system sends a driving burst signal of 8 cycles, which typical voltage of 400 V, to the transmitting EMAT (T-EMAT) via a diplexer. This diplexer allows a unidirectional feed from the system to the EMAT and prevents the feedback signal. The T-EMAT then generates a particular torsional mode, depending on the driving frequency and the periodicity of the PPM-EMAT. The propagating waves are detected by the receiving EMAT (R-EMAT) or a needle-piezoelectric transducer and sent back to the system after being pre-amplified. The matching impedance is required when an EMAT is used in the receiving side. All the measurement parameters, including the operation frequency, the burst duration time, the amplification gain and the integrator gate, are set through a personal computer. As mentioned before, the proposed method relies on a traveling time measurement. This is done by gating out the intended signal displayed in the oscilloscope to obtain the phase-shift dependence of the frequency. Figure 3.2 illustrates this procedure, where the signal in (a) is gated and the frequency-phase relationship is obtained (b) by using a home-built PC program. The gate is shown with red color in (a).

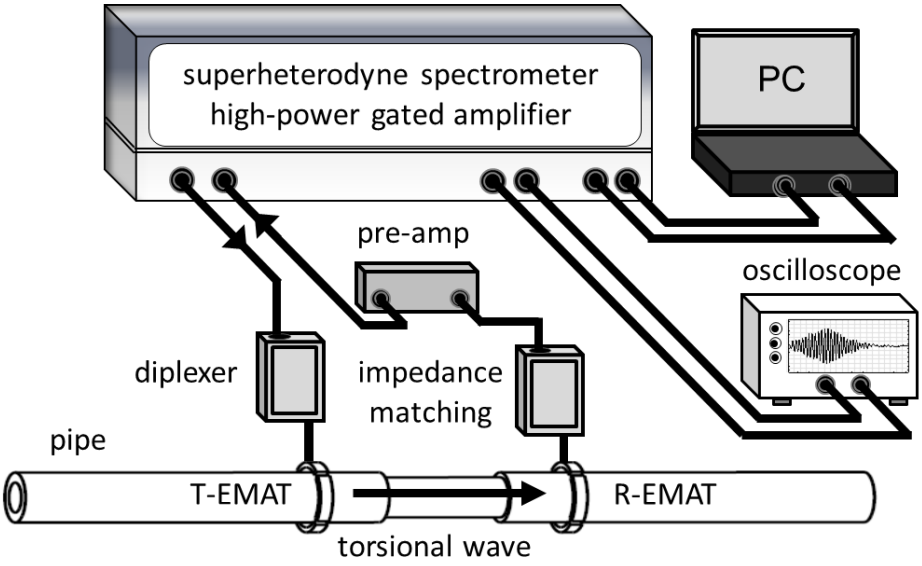

Figure 3.1 Typical experimental setup and the placement of EMATs around the pipe.

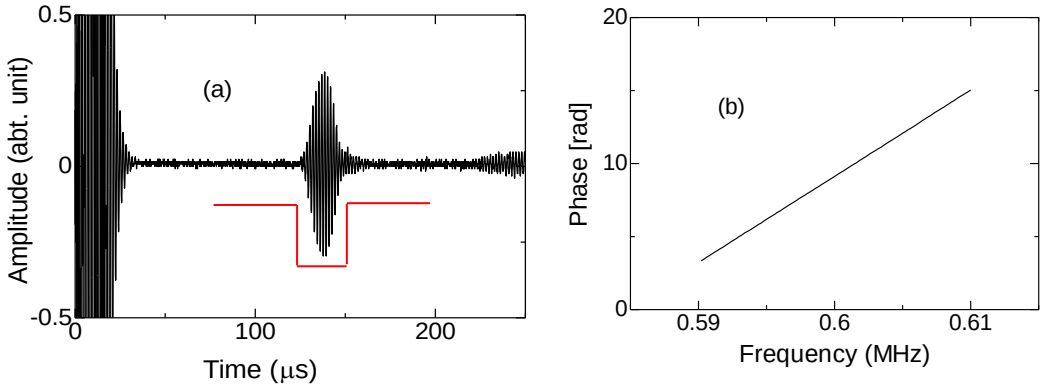

Figure 3.2 Traveling time determination from a waveform (a) and the measured phase-frequency relationship, from which the traveling time can be obtained (b). The gate is shown by a red line.

3.3 Concept of Mode Conversion

As previously mentioned, every higher mode of torsional waves is dispersive, meaning that the velocity depends on frequency and thickness of the waveguide, in addition to the material itself. The dispersion curves of T(0,1) and T(0,2) modes, relating frequency×thickness and group velocity, is shown once again in Fig. 3.3. The group velocity of a T(0,1) mode is constant at all frequency×thickness, which is equal to the shear wave velocity of the material. However those of a T(0,2) mode is affected by frequency×thickness, especially at a low-frequency range. When the frequency is fixed, the group velocity depends solely on the thickness. The group velocity decreases as the thickness decreases, as illustrated by the red line, and it becomes zero when the thickness is equals to the cut-off thickness. In order to keep propagating, the mode should convert into a lower T(0,1) mode, causing a group velocity jump. This group velocity dependence on group velocity can be a basis for wall-thinning inspection and this is the main idea in the present study. The use of EMAT with a fixed wavelength enables the implementation of this idea.

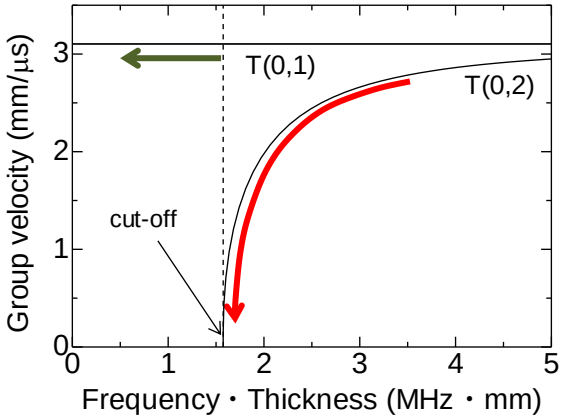

Figure 3.3 Group velocity dispersion curves of torsional modes propagating in a 3-mm thick aluminum pipe (c_s = 3.1 mm/μs) with diameter 25 mm.

3.4 Observation of Group Velocity Dependence on Thickness

3.4.1 Introduction

The objective of the first fundamental study is to observe a thickness dependence of group velocity. The T(0,1) and T(0,2) modes are generated in several pipe specimens containing defects and the propagating waves are detected by another identical EMAT. A circumferential reduction in outside diameter over a length of 200-mm was introduced in the center of each specimen. They have different remaining thicknesses at their thinning regions, which are located between the two EMATs. These EMATs are separated by 400 mm in every measurement and the traveling time for that distance is measured. Figure 3.4 illustrates the EMATs placement and defect location on the pipe. Firstly, the aluminum pipes are used as specimens. The experiment is then repeated with steel pipe specimens.

The traveling time of T(0,1) mode generation should be independent of the thickness while that of T(0,2) mode is expected to be affected by the thickness change. This study focuses on group velocity change which is caused by mode conversion. To confirm this conversion, group velocity in the thinning region is determined from the measured traveling time of each mode generation. Traveling time in the specimen without a thinning region is used to determine the experimental group velocity in the defect-free part. The traveling time through only the thinning region is then obtained by subtracting the measured traveling time. Because the axial length of the thinning region is known, the group velocity in this region can be calculated. The theoretical dispersion

relation is used to interpret the change in group velocity. The experimental group velocity is then plotted against the calculated dispersion curves relating the frequency×thickness versus group velocity. The group velocity of the T(0,1) mode is expected to be constant in all the range of frequency×thickness while that of T(0,2) mode should vary following the thickness change.

3.4.2 Aluminum pipe

a. T(0,1) mode generation

T(0,1) mode is generated at a frequency of 0.615 MHz in aluminum specimens. The typical received waveforms in defect-free and defective pipes are shown in Figs. 3.5(a) and (b), respectively. The remaining thickness at defect in (b) is 1.8 mm. The thickness change induces reflection at defect's edge; therefore the transmitted amplitude is observed to be smaller in the specimen with defect. Further investigation reported in section 3.6 discovers that this reflection is affected by the rate of thickness transition slope at the edge.

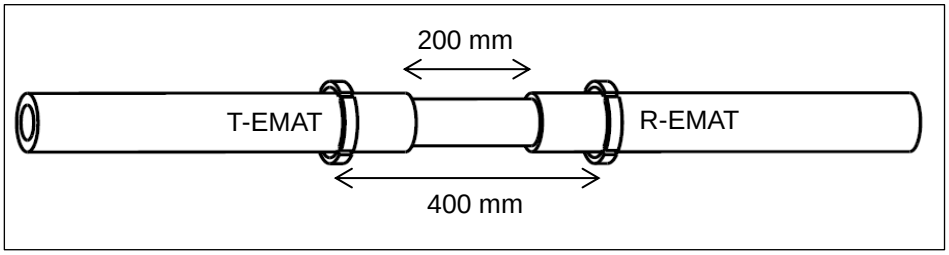

Figure 3.4 EMATs placement around the pipe with the defect located between them.

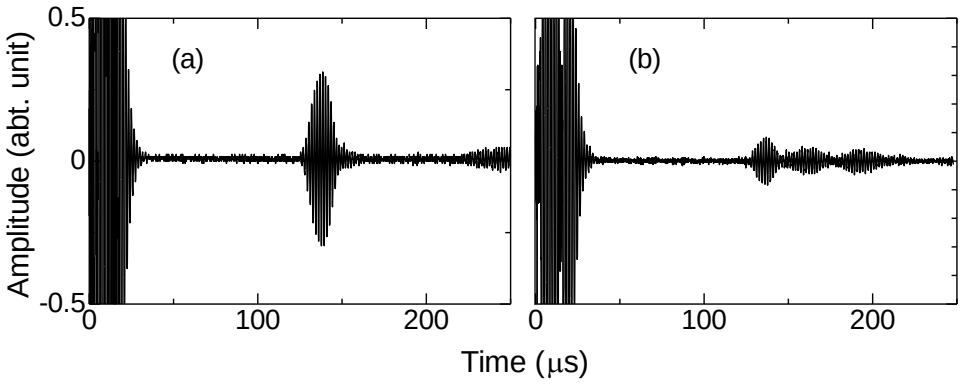

Figure 3.5 Received waveforms when T(0,1) mode is propagated in a defect-free aluminum pipe (a) and defective pipes with 1.8 mm remaining thickness at the defect.

By gating out the intended signal and measuring the phase dependence of frequency, the traveling time is obtained. Figure 3.6(a) presents the traveling time of T(0,1) mode generation in the specimens of the same traveling distance. The horizontal axis is the remaining thickness at the defect of each specimen. This is the as-measured traveling time associated with the total distance between the transmitting and receiving EMATs, which includes the defect-free region. The T(0,1) mode takes nearly the same time regardless of the varying depths of defects. Group velocity at the defect is obtained through the procedure explained in section 3.4.1. Comparison of this group velocity with the theoretical dispersion curves is presented in Fig. 3.6(b). The group velocities in the thinning region appear to equal the shear wave velocity in aluminum (3.1 mm/μs). No significant variation is observed for varying thickness, indicating that no mode conversion occurs. This result confirms the non-dispersive nature of the fundamental T(0,1) mode; the group velocity is independent of thickness and frequency.

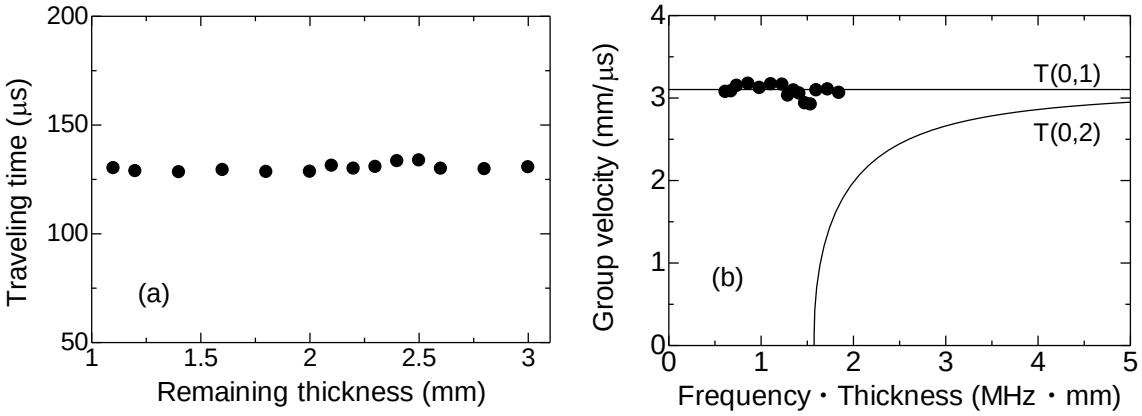

Figure 3.6 Traveling time (a) and the observed group velocity of T(0,1) mode generation in different thicknesses plotted against the theoretical dispersion curves (b) [55].

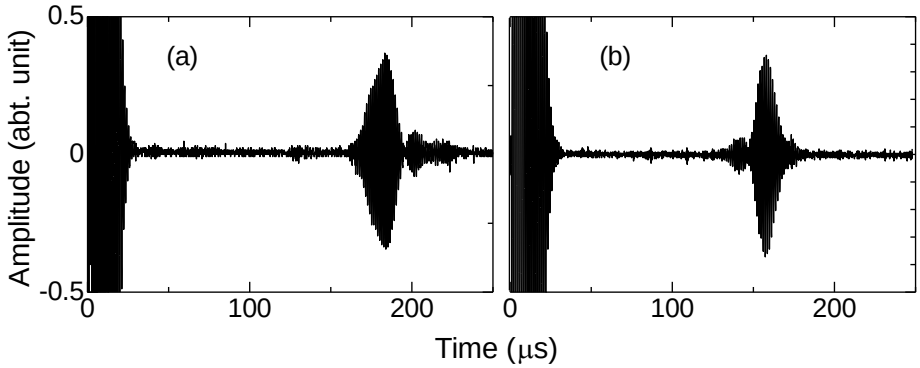

Figure 3.7 Received waveforms when T(0,2) mode is propagated in a defect-free aluminum pipe (a) and defective pipes with remaining thickness 1.8 mm.

b. T(0,2) mode

T(0,2) mode is generated in aluminum pipe at a frequency of 0.77 MHz. Figure 3.7 shows the waveforms of this mode generation in the same specimens as in Fig. 3.5. Relationship between the depth of defect and amplitude for this mode is not as straightforward as that of T(0,1) mode. This is because conversion to T(0,1) mode is involved, as will be discussed soon. Amplitude of this mode alone cannot be used to evaluate a defect.

Figure 3.8(a) shows the measured traveling time when T(0,2) mode is excited. The theoretical cut-off thickness of T(0,2) mode is indicated by the dashed line. The observed traveling time suddenly drops in all specimens with the remaining thickness equals to or smaller than 2.3 mm. This indicates mode conversion of T(0,2) mode into lower T(0,1) mode, which possesses a higher group velocity in the thinning region. Comparison with the theoretical dispersion curves is presented in Fig. 3.8(b). The group velocity of T(0,2) mode is highly affected by the thickness (note that the frequency is fixed). In the first five specimens with thicker remaining thicknesses, the group velocity decreases as the thickness decreases and fits very well with the theoretical dispersion curve for T(0,2) mode. However, the group velocities in the rest of the specimens are higher, being close to the shear wave velocity. It means that the generated T(0,2) mode converts to lower T(0,1) mode when the thickness is smaller than a certain value, which is supposed to be the cut-off thickness.

This result experimentally verifies the presence of the cut-off thickness of T(0,2) mode, below which this mode cannot exist and converts into T(0,1) mode. The discrepancy between the theoretical cut-off thickness (2.1 mm) and the one obtained by experiment (2.3 mm) is probably caused by thickness measurement errors. Below the cut-off thickness, the pipe-wall cannot support the asymmetric vibration of T(0,2) mode across the thickness, so that it converts to a uniform vibration belonging to the lower T(0,1) mode. More discussion on this is covered in the section 3.5.

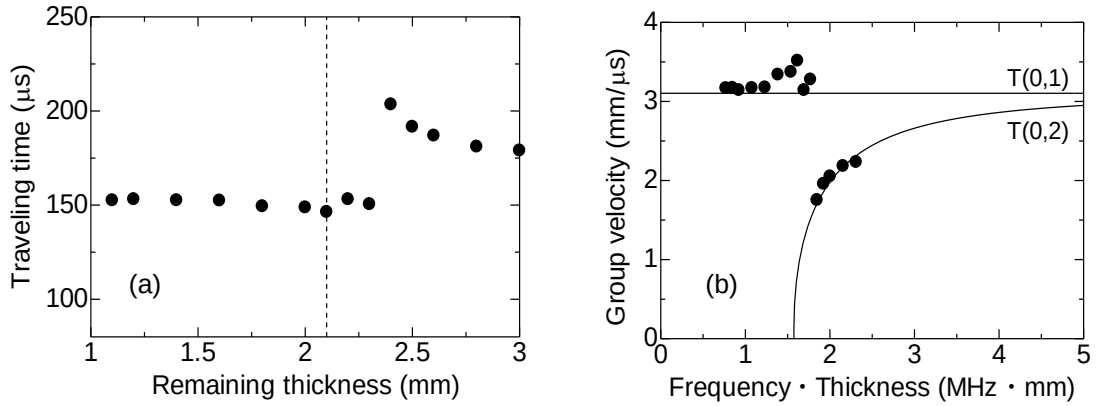

Figure 3.8 Traveling time (a) and the observed group velocity of T(0,2) mode generated in aluminum with different thickness, plotted against the theoretical dispersion curves (b) [55].

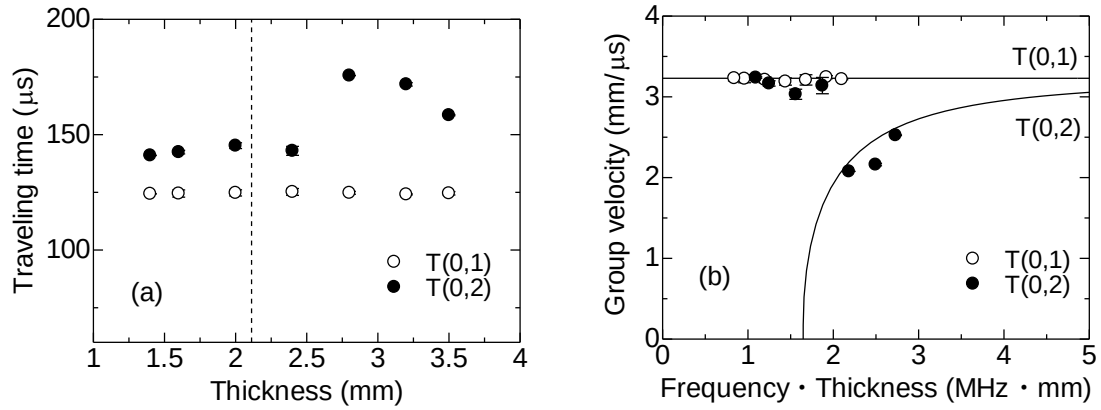

Figure 3.9 Observed traveling time (a) and group velocity dependence (b) on thickness of torsional mode generation in steel pipes, compared against the theoretical dispersion curves.

3.4.3 Steel pipe

The same investigation of group velocity dependence on thickness is performed with steel pipe specimens. In these specimens, the T(0,1) and T(0,2) modes are generated at frequencies of 0.60 and 0.78 MHz, respectively. The traveling time and group velocity dependence of each mode is presented in Fig. 3.9. Basically, similar results are obtained as those in aluminum pipes – as expected. The traveling time and group velocity of the T(0,1) mode is independent of thickness due to its non-dispersive characteristic. When the thickness is larger than the cut-off thickness, the group velocity of T(0,2) mode decreases as the thickness decreases, showing a good agreement with the theoretical dispersion curves. A jump in group velocity is observed

when the thickness is smaller than cut-off thickness, indicating a conversion to T(0,1) mode.

3.5 Mechanism of mode conversion

3.5.1 Introduction

In the previous experiment reported in section 3.4, a pitch-catch measurement using two EMATs was carried out to measure the traveling time of torsional modes propagating in pipes with a defect (a thinning region). It was found that the traveling time of a higher torsional mode changed depending on the depth of the thinning and the result indicating the mode conversion was achieved. On the basis of this finding, further experimentation is performed to investigate the mechanism of this mode conversion.

Aluminum pipe is used as a specimen in this experiment. The pipe is 1000 mm in length with inner and outer diameters of 19 and 25 mm, respectively (3 mm wall thickness). A specimen with a defect is prepared in addition to a defect-free pipe as a reference. The defect causes a thinning region in the whole circumference, which lies 200 mm in the axial direction and has a remaining thickness of 1 mm (less than the cut-off thickness of T(0,2) mode). In this experiment, a needle-type piezoelectric transducer (called a pinducer) replaces the R-EMAT in the receiving side shown in Fig. 3.1. This transducer is used because it can detect multi-modes at every scanning point. The multi-modes detectability is required in this experiment to investigate the detail mechanism of mode conversion. The T(0,1) and T(0,2) modes are generated and the receiver is moved in increments of 5 mm along the 400 mm length of the pipe to detect and record the propagating waves. The measurement site includes the defect-free regions before and after the thinning region and the defect region itself, as illustrated in Fig. 3.10.

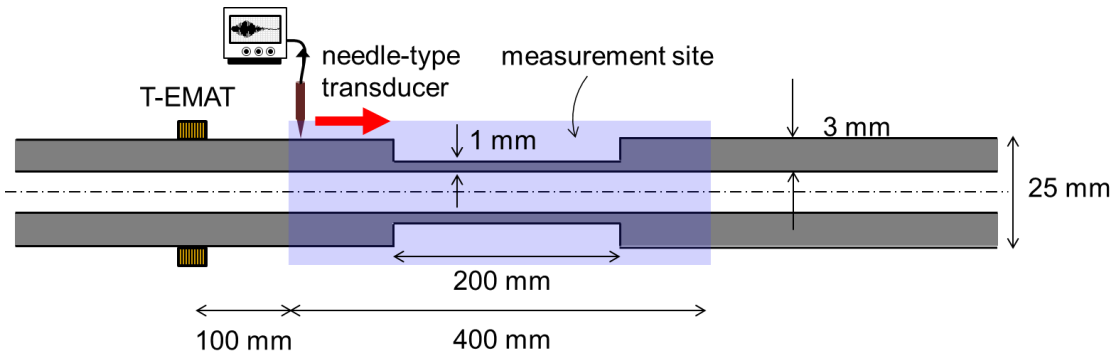

Figure 3.10 Cross section of the pipe scanned by a pinducer as the red arrow indicates.

3.5.2 T(0,1) mode generation

The received waveforms of T(0,1) mode generated, as identified by the three different positions shown in Fig. 3.11, are presented in Fig. 3.12. The intended signal being focused is the direct (the first arrival) signal. The amplitude of this signal decreases from (a) to (c), which is related to the traveling distance and reflection at the edge(s). Figure 3.13 explains the origin of each signal in Fig. 3.12(a).

The traveling time of the intended signal at each location is deduced by gating it out from the received signals in Fig 3.12 and presented in Fig. 3.14(a). This figure relates the distance from the transmitting EMAT and the propagating time such that the slope corresponds to the inverse of the group velocity. The defect is confined between the dashed lines in this figure and the obtained group velocity in each region is also presented. The group velocity in the thinning region (1 mm thick) is 3.11 mm/μs, which is almost the same as the velocity of 3.17 mm/μs for the original thickness (3 mm). The theoretical velocity of this fundamental mode is equal to the shear wave velocity, which is 3.1 mm/μs for aluminum. This observation indicates that the T(0,1) mode continues to travel through this region. However, when the thickness returns to the original at the far end, the observed velocity is 1.8 mm/μs, which is smaller than those measured before and within the defect. The calculated group velocity of the T(0.2) mode at frequency 0.615 MHz is 1.7 mm/μs. It then can be concluded that the generated T(0,1) mode converts to the higher T(0,2) mode. The mechanism of this conversion can be explained by the displacement redistribution as in the case of SH guided waves [37]. Figure 3.15 illustrates this; it shows cross-sectional side view of the pipe and the displacement distribution of the torsional modes. In cases where the thickness increase is more than double after the defect, now from 1 to 3 mm as described previously, it is easier for T(0,1) mode to propagates as T(0,2) mode. Comparison between this experimental result and the theoretical dispersion curves is presented in Fig. 3.14(b). The frequency is fixed at 0.615 MHz, which is the same as that in the experiment, and the horizontal axis is the thickness of the specimen. The numbered arrows indicate the sequence of change in the measured group velocity in relation to the change in thickness.

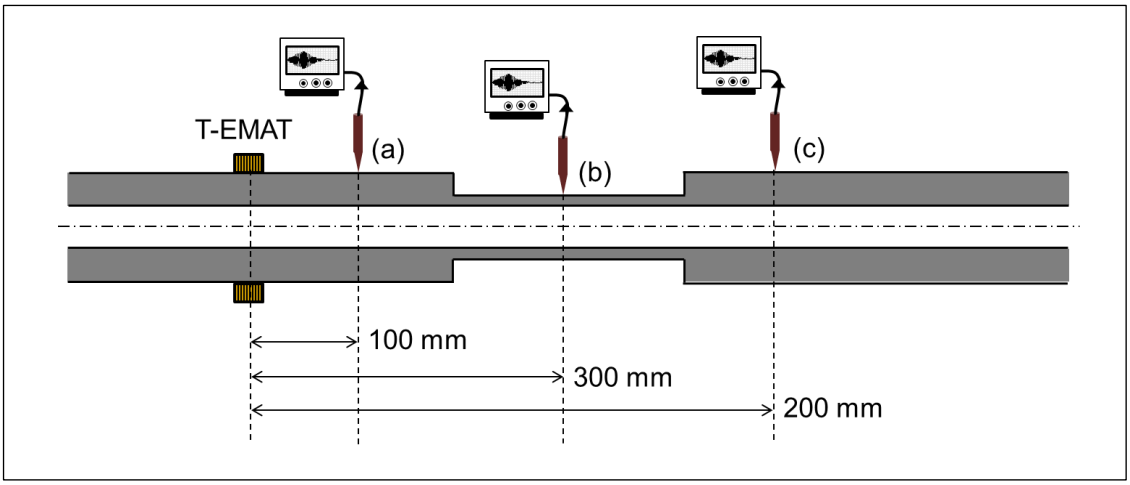

Figure 3.11 Three different positions at where the Figs. 3.12 and 3.16 are obtained.

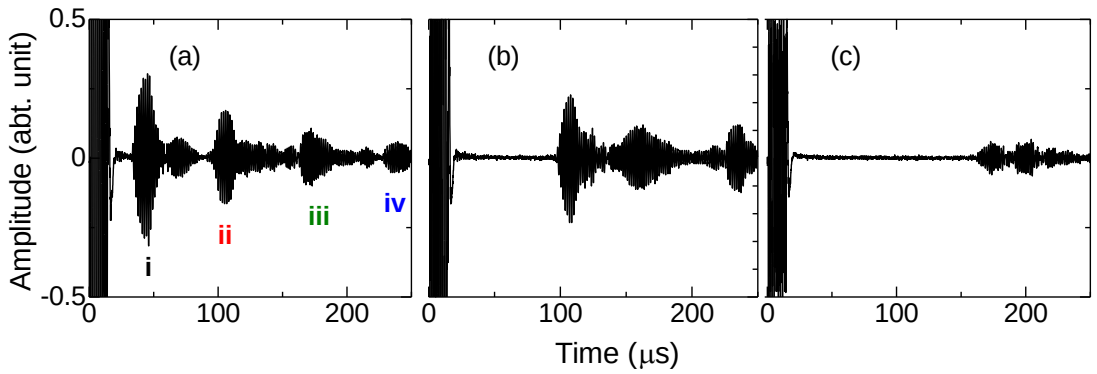

Figure 3.12 The waveforms of T(0,1) mode generated which are detected at defect-free region (a) at the defect (b) and after the defect (c).

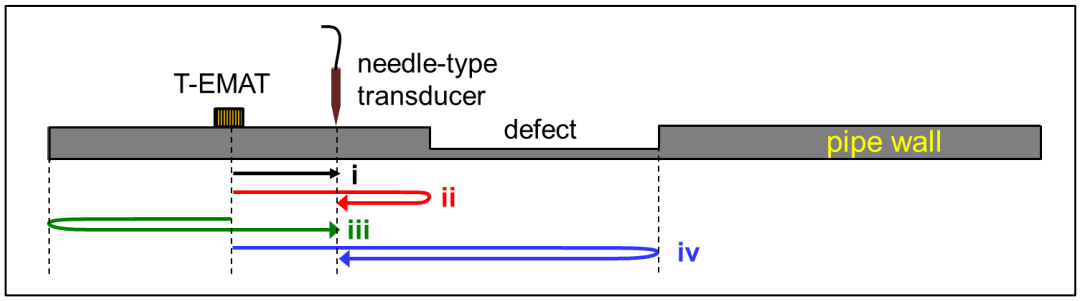

Figure 3.13 Traveling paths of the waves detected before the defect.

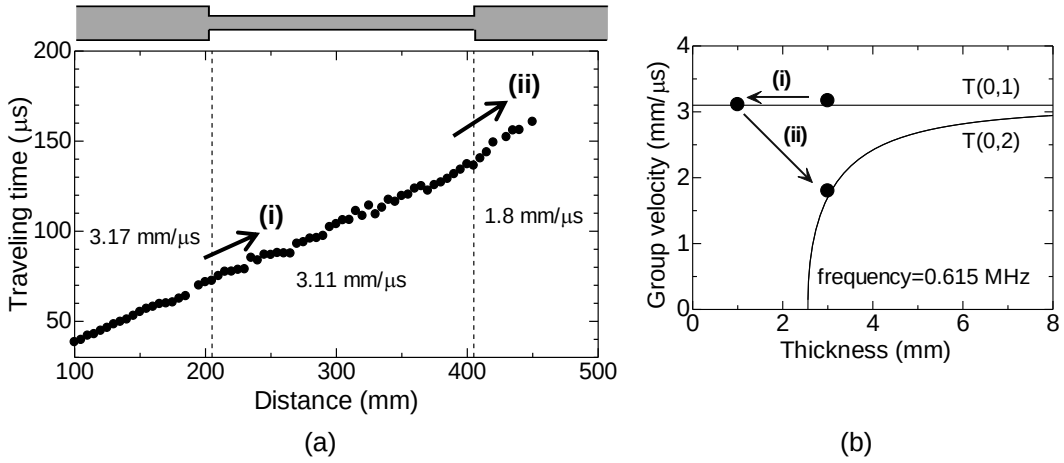

Figure 3.14 Traveling time for T(0,1) mode generated after propagating for different distances (a). The slope of time versus distance gives the group velocity at each region, which is compared with the theoretical dispersion curves at a fixed frequency of 0.615 MHz (b). The numbered arrows indicate the sequence of mode conversions following the thickness change [56].

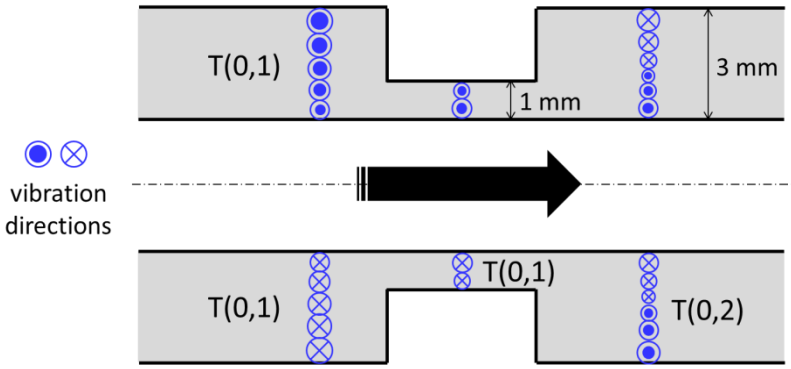

Figure 3.15 Cross sectional side view of the pipe showing the mode conversion of T(0,1) mode after defect. Arrows shows the propagation direction. The relative thickness is exaggerated.

3.5.3 T(0,2) mode generation

Figure 3.16 shows the waveforms when the T(0,2) mode is generated. They are detected at the locations identified in Fig. 3.11; before the defect in (a), at and after the defect in (b) and (c), respectively. Traveling time at each point of measurement is presented in Fig. 3.17(a). The observed group velocity before the defect is 2.06 mm/μs. It becomes 3.11 mm/μs in the thinning region, which indicates a conversion to the T(0,1) mode. When the thickness returns to 3 mm after the defect, the group velocity becomes 2.49 mm/μs. This observed group velocity is between those for the T(0,1) and T(0,2) modes (3.11 and 2.06 mm/μs). Therefore, this velocity change indicates that the T(0,1) mode converts back to the T(0,2) mode while a part of the T(0,1) mode remains, resulting in interference between the two signals. This interference is clearly observed in the assortment of received waveforms that will be presented in the section 3.6.

Figure 3.17(b) shows a comparison of this experimental result with the theoretical dispersion curves for a fixed frequency of 0.77 MHz, which shows group velocity dependence on thickness. The first conversion from the T(0,2) mode to the T(0,1) mode takes place when the thickness reduces from 3 to 1 mm, indicated by arrow (i). Conversion back to the T(0,2) mode occurs when the thickness returns to 3 mm [arrow (ii)]. Figure 3.18 illustrates this mechanism of mode conversion, showing vibrational directions in cross-sectional view of the pipe.

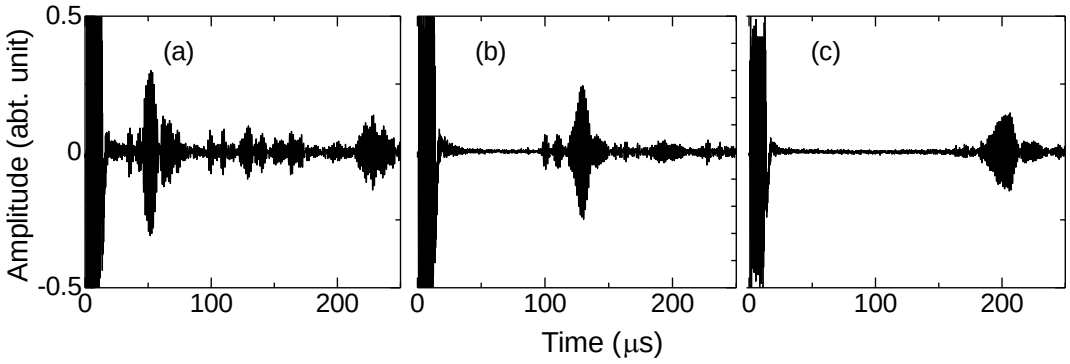

Figure 3.16 The waveforms of T(0,2) mode generation which are detected at defect-free region (a) at the defect (b) and after the defect (c).

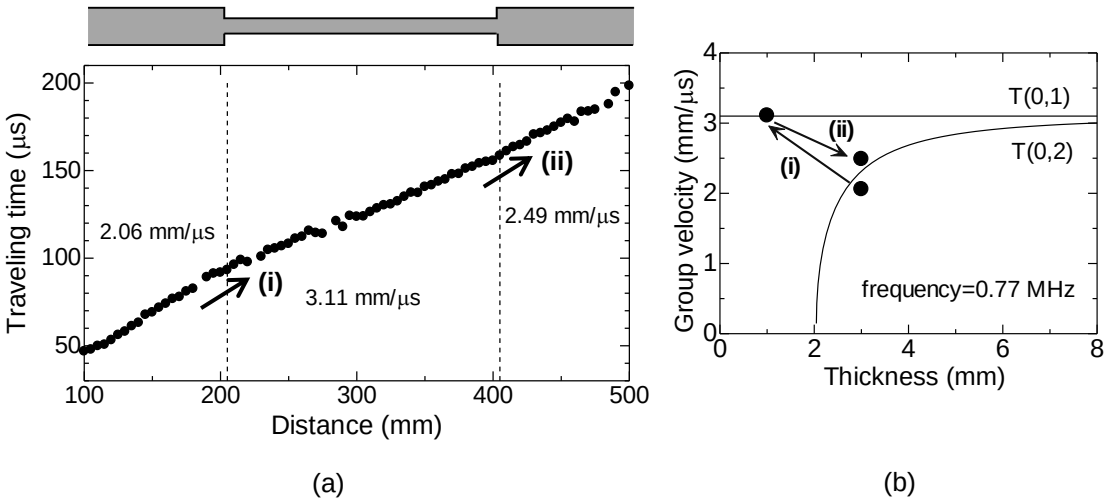

Figure 3.17 Observed traveling time at different distance of the T(0,2) mode generated (a), and the comparison with the theoretical dispersion curves with a fixed frequency at 0.77 MHz (b) [56].

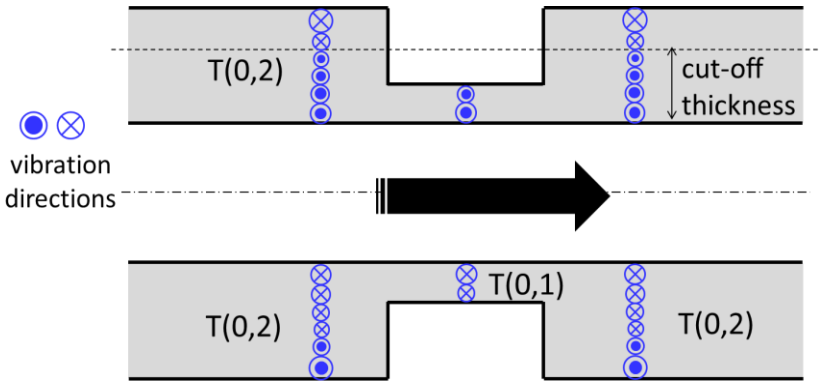

Figure 3.18 Cross sectional side view of the pipe with an exaggerated thickness, showing mode conversion mechanism of T(0,2) mode. Propagation direction is indicated by the arrow.

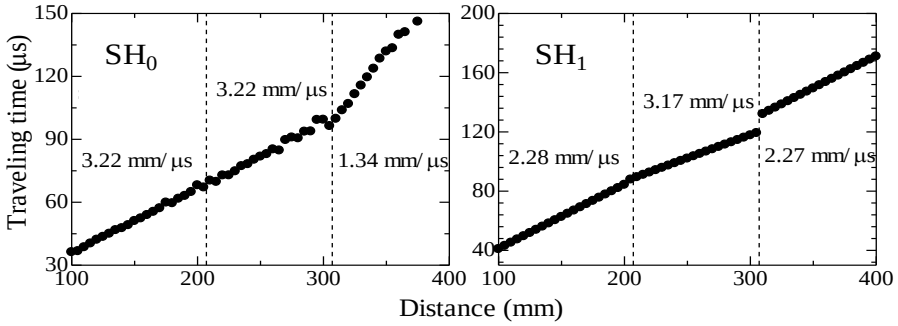

Figure 3.19 Mode conversion of SH guided waves propagating in a defective aluminum plate. The defect is located between the dashed lines [36].

3.5.4 Similarity with the SH guided waves

The mode conversion behavior of T(0,1) and T(0,2) modes are similar to those of the fundamental and the first higher modes of shear horizontal guided wave, SH_0 and SH_1 modes, propagating in a plate waveguide. Figure 3.19 shows the mechanism of mode conversion for SH guided waves when each mode is propagated in a 3 mm-thick plate containing a defect [36]. The remaining thickness at the defect is 1 mm, being smaller than the cut-off thickness of the SH_1 mode. The defect is confined between the dashed lines. This similarity can be expected since these two waves are essentially identical. They belong to the family of shear wave whose vibrations are parallel to the surfaces. In fact, the dispersion relation for a torsional wave propagating in a pipe with a small thickness-diameter ratio (big thin pipe) can be approximated as that for an SH wave.

3.6 Mode Conversion in Tapered Defect

3.6.1 Specimen

Observation of mode conversion reported in the previous section uses pipes containing step-like defects as specimens. In these specimens, the thickness abruptly changes at the edges. Most actual wall-thickness reduction areas have a rather smooth edge, such as a dent or depression [58]. Therefore it is also important to investigate the conversion behavior when the thickness change is gradual. Pipes of aluminum alloy A5052 are prepared as specimens for this investigation. Thinning regions are introduced at the center of them. This region lies 200 mm in the axial direction and has a remaining thickness of 1 mm in all specimens.

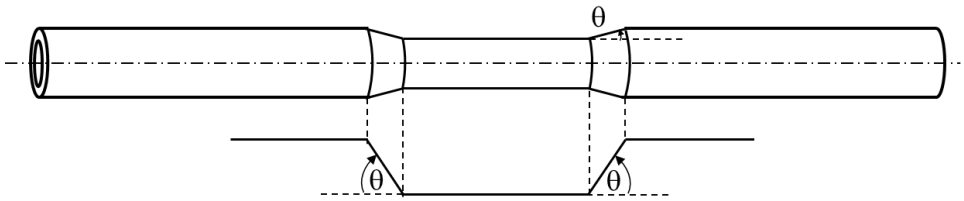

Figure 3.20 Pipe with a tapered defect

This thickness is smaller than the cut-off thickness of T(0,2) mode. The thinning regions cover the whole circumference and differ by the sloping degree at the edges. In addition to the specimen with 90° slope of the defect edge (step-like edge), four specimens with different diametrical transitions are prepared: 30°, 20°, 10°, and 5° slopes (from horizontal); that is, the specimen with the 5° sloping edge has the longest tapered area. Figure 3.20 illustrates the pipe specimen with such a defect.

3.6.2 Observation of propagation behavior [56]

The T(0,1) and T(0,2) modes are generated in aluminum pipe specimens by an EMAT and detected by a needle-type piezoelectric transducer. The receiver is moved every 5 mm to pick up the propagating waves in the same way as the experiment reported in section 3.5. The same procedure is repeated in every specimen. Figures 3.21 and 3.22 are assortments constructed from the received waveforms, similar to those shown in Figs. 3.12 and 3.16, obtained at many scanning points for each mode generated in different specimens. From top to bottom, the figures are taken from specimens with edges of 90° (step-like edge), 30°, 20°, 10°, and 5° inclinations. The shape of the edge is illustrated on the top of each figure for easier understanding. The defect is confined between the dashed lines. These figures relate the distance from the transmitting EMAT and the propagating time such that the slope corresponds to the inverse of the group velocity. The intended signal being focused is the direct (the first arrival) signal.

The T(0,1) mode is excited at a frequency of 0.615 MHz. Figure 3.21 reveals that this mode is less reflected when the thickness transition at defect's edge is smoother. The traveling time of the direct signal in every distance in the specimen with a step-like edge [Fig. 3.21(a)] is investigated to obtain the group velocity which results are reported in section 3.5.2. As shown in Fig. 3.14(a), the observed group velocities are 3.17, 3.11 and 1.8 mm/μs, before, through and after the defect, respectively. Mode conversion of T(0,1) to T(0,2) is observed when the thickness increases after the defect. This conversion into a higher mode is not observed in the case of specimens with a smoother thickness change at the defect edge.

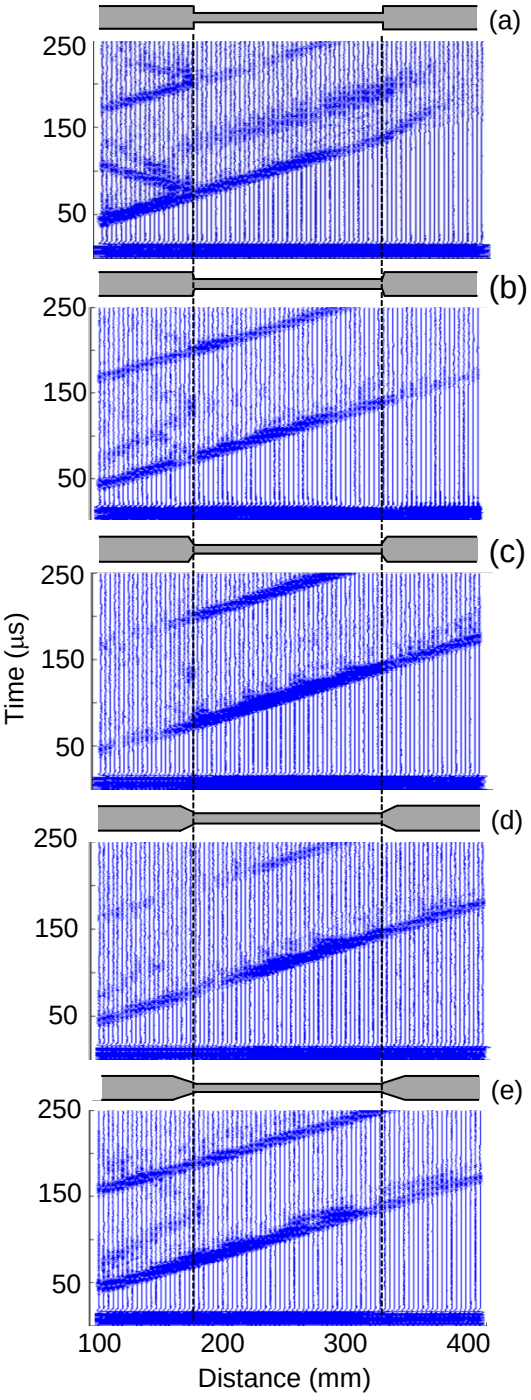

Figure 3.21 Wave propagation of T(0,1) mode generated in specimens with edge angles of (a) 90°, (b) 30°, (c) 20°, (d) 10° and (e) 5°. Edges of the thinning region are indicated by broken lines.

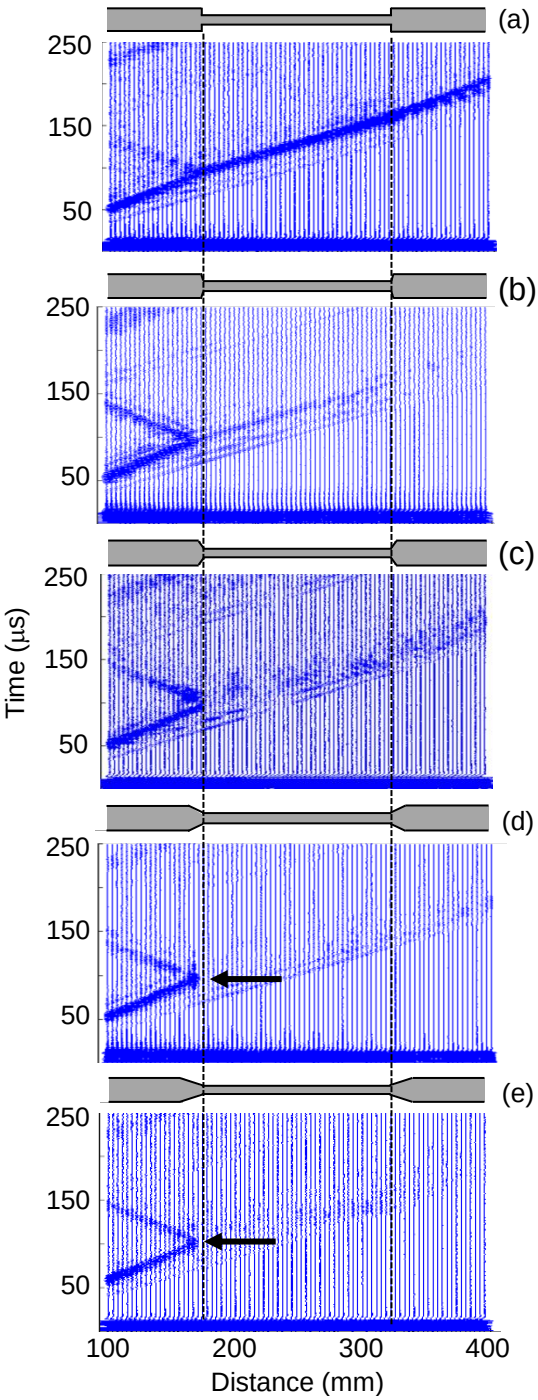

Figure 3.22 Wave propagation of T(0,2) mode generated in the same pipes used to obtain Fig. 3.21. Arrows show the total reflection in (d) and (e).

In the specimen with a gradual transition, the wave cleanly propagates into the region with defect. This experimental finding agrees with the simulation performed by Carandente *et al* [57]. They predicted the reflection coefficient of the T(0,1) mode when it is propagated in a tapered defect. They used the ratio of the midpoint length of the tapered region to the wavelength as the parameters. With these parameters of the current experiment, it was reported that the reflection coefficient decreases with the slope angle.

The shape of the edge transition affects the propagation behavior of the T(0,2) mode in an opposite manner. As the thickness change becomes smoother, the signal reflection becomes clearer, as can be observed in Fig. 3.22. Furthermore, a total reflection of the generated signal is observed in the last two specimens with very gentle thickness transitions (sloped by 10° and 5°), as shown in the Figs. 3.22(d) and 3.22(e). The entire wave is reflected back and there is no transmission at all through the defect. The arrows in these figures indicate the location where the total reflection occurs, which corresponds to a thickness of 1.87 mm. This point is located within the sloping region and close to the theoretical cut-off thickness of the T(0,2) mode, which is 2.1 mm.

The total reflection behavior was also observed when the first higher mode of the shear horizontal guided wave (SH_1) mode was propagated in a plate specimen [38]. Figures 3.23(a-c) show simulation results of SH_1 mode propagation represented in cross-sectional side view, taken at different time sequentially: 55, 75, and 80 μs, respectively. The sloping angle at defect is 5° and the thickness of the plate is exaggerated for convenience of explanation. The dashed line in Fig. 3.23(a) indicates the generation site while black arrows denote the propagation directions. The generated wave propagates in both directions and the total reflection occurs at the sloping region, leaving no transmitted wave through the defect. Detailed analysis of wave propagation at the sloping region reveals that the wavenumber is changing in this region. This wavenumber modification is corroborated with the theoretical dispersion curves and presented in Fig 3.23(d). The wavenumber decreases as the thickness decreases, being in a good agreement with the dispersion curve, and it reaches zero at the cut-off thickness, causing a total reflection of the incident wave.

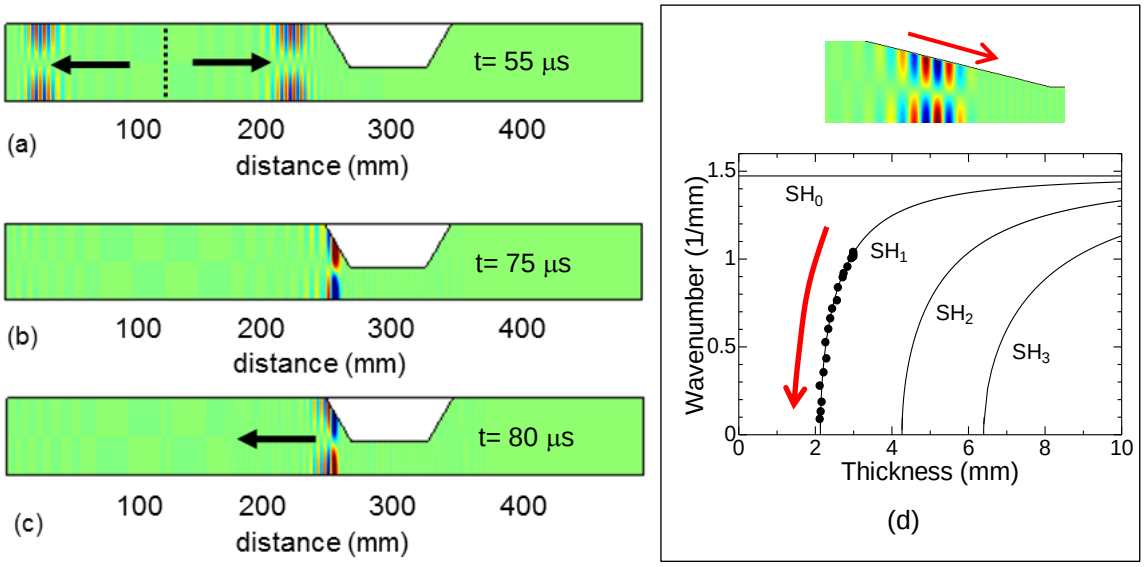

Figure 3.23 Numerical simulation of the SH_1 mode propagating in a plate containing tapered defect, showing a total reflection (a-c) and wavenumber modification at the sloping region (d) [37]. Detail propagation at the slope is shown as the inset.
Red arrows show the path of wavenumber change.

3.6.3 Tapered defect in a steel pipe

Propagation behavior reported in the previous section should apply to any material. To confirm this, a simple experiment is performed with two steel pipes, each containing a defect. The defect has a step-like edge in the first specimen and a tapered edge with sloping angle 5° in the second. Two EMATs are used as transmitter and receiver. They are separated by 400 mm with the defect located between them. Figure 3.24 shows the received waveforms for T(0,1) mode generation in the those specimens, followed by Fig. 3.25 for T(0,2) mode generation. The intended signals are indicated by oval marks.

The received waveform of T(0,1) mode generation in specimen with a tapered defect apparently has a larger amplitude compared to that in specimen with a step-like defect. It indicates that the mode has a bigger transmission coefficient (less reflected) when the thickness transition is smoother. An opposite behavior is observed for the T(0,2) mode generation. The T(0,2) signal is barely observed in the specimen with a tapered edge, indicating that there are almost no

transmission through the defect. It can then be estimated that the generated mode is totally reflected somewhere between the generating and receiving EMATs. These behaviors of the two modes are indeed consistent with the results obtained with aluminum pipes reported in the previous section.

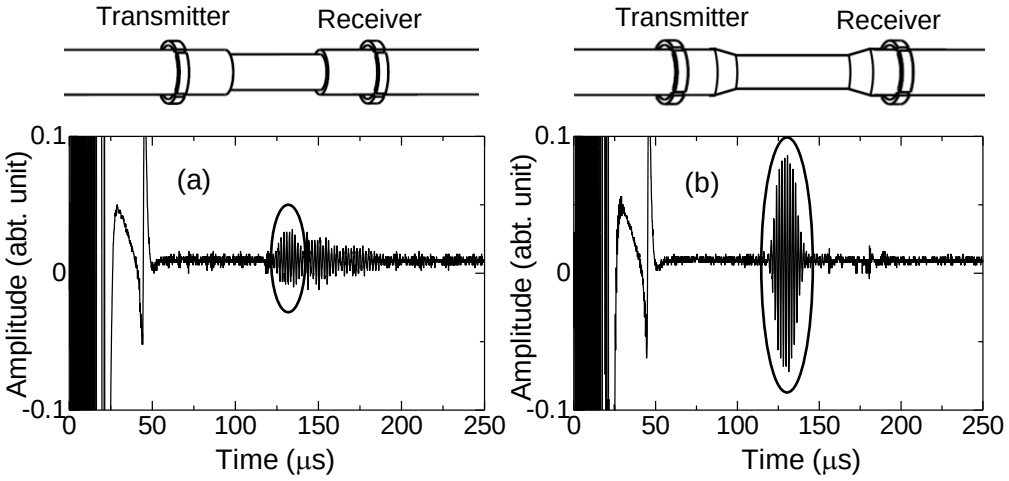

Figure 3.24 Received waveforms when T(0,1) mode is generated in steel pipe with defects. The defect has step-like edges in (a) and tapered edges in (b). The intended signals are indicated by oval marks.

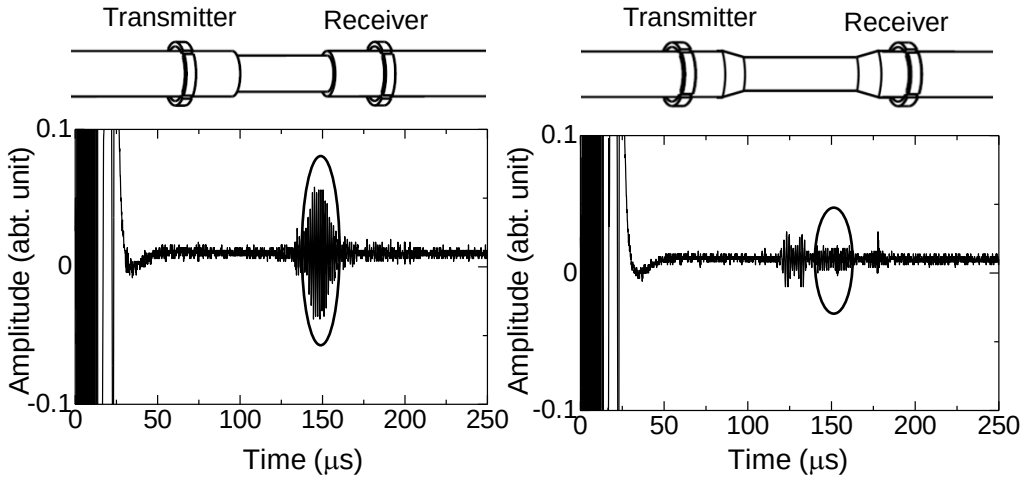

Figure 3.25 Received waveforms when T(0,1) mode is generated in the same defective steel pipes as in Fig. 3.24. There is no observed signal in the specimen with a tapered edge (b), indicating a total reflection at the tapering edge.

CHAPTER IV

APPLICATIONS

4.1 Introduction

This study proposes a new method for pipe inspection based on group velocity change of torsional waves caused by mode conversion. When a higher mode of torsional wave is propagated in a pipe, its group velocity highly depends on the frequency and thickness of the pipe. The group velocity will decrease as the frequency×thickness decreases. By maintaining the frequency at a fixed value, the group velocity is then a function of only the pipe thickness. Every higher mode has a critical thickness where the waveguide cannot support the propagation of the associated mode. In this situation, the mode should convert to a lower mode in order to continue propagating. This conversion causes a significant jump in the group velocity. The current study attempts to use this behavior as the basis for wall-thinning inspection of pipe. With this proposed method, the frequency has to be at a fixed value throughout the whole measurement. The use of electromagnetic acoustic transducer (EMAT) enables this requirement and provides a noncontact measurement method at the same time.

Some fundamental studies to support the proposed method have been reported in chapter III. The fundamental T(0,1) and the first higher T(0,2) torsional modes were propagated in several aluminum and steel pipes containing defects. The thickness dependence of group velocity was then experimentally observed and the results were interpreted using the theoretical dispersion curves. It was confirmed that the group velocity of the T(0,1) mode is thickness independent, while that of the T(0,2) mode is highly influenced by thickness change and as a result, mode conversion was observed in some situations. It was also found that the shape of the edges of the defect significantly affects this conversion behavior.

In this chapter, some applications of the proposed method are reported. Several pipes containing various kinds of defects are inspected. The inspection is carried out from the outer-side of the pipe. However, many actual pipe inspections are done from the inside of the pipe, which uses a measurement tool (the so-called PIG) that moves inside the pipe, taking advantage of the flow of the transported fluid within the pipe. To cope with this needs, a pair of special EMATs are

developed, which can be used from inside the pipes to perform inspection. Some experiments are also carried out with this internal EMAT. The measurement setup for all experiments is identical with that shown in Fig. 3.1.

4.2 Outside Inspection

4.2.1 Partially circumferential defects

The first application, with a pair of outside EMATs, is to inspect pipes containing partial-circumferential defects. Figure 4.1 illustrates the specimen and the placement of EMATs and the cross section view at a defective region. The axial length of the defect is 200 mm with step-like edges and constant wall thickness in the thinning region. In every specimen the remaining thickness at the site of the defect is the same, which is 1 mm in aluminum and 1.2 mm in steel specimens, being smaller than the cut-off thickness of the T(0,2) mode; therefore, this mode should convert to the T(0,1) mode at this region. The conversion is observed as a group velocity change, which causes a decrease in the measured traveling time. The defect does not cover the entire circumference of the pipe and the length of defect in the circumferential direction, L, is different in each specimen. This variant is introduced to enable measurement of defects with different cross-sectional losses. Two EMATs are used as transmitter and receiver. A fixed distance of 400 mm separates them with the defect located between them. In practical applications using the proposed method, both the transmitter and receiver sides should be EMATs, so that a noncontact measurement is possible. In addition, by using an EMAT as a receiver, it is possible to detect only the intended mode at a fix frequency. The T(0,1) and T(0,2) modes are propagated in aluminum or steel pipe specimen and the traveling times are measured to determine the group velocity at defect.

a. Aluminum pipe

The observed group velocity at a defect when T(0,1) and T(0,2) modes are propagated in defective aluminum pipes is presented in Fig. 4.2 as a function of the ratio of the cross-sectional area loss with respect to the original defect-free pipe. A full-circumferential defect reduces the cross section of an original defect-free area by 69.7%. As a reference, the group velocity for each mode propagating in a defect-free specimen (0% cross sectional loss) for the same distance is also included.

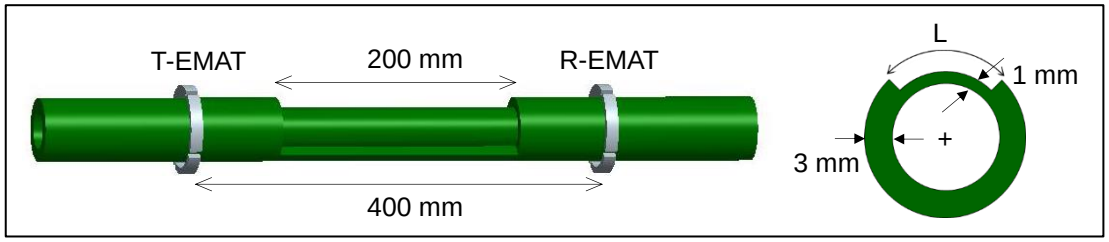

Figure 4.1 Pipe specimen with a circumference partial defect and the placement of EMATs on it and cross-sectional view at a defective region with L indicates defect circumferential length

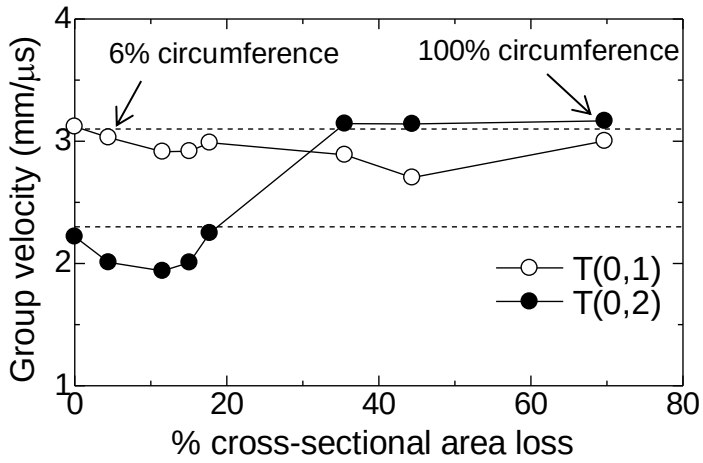

Figure 4.2 Group velocity at defect of the two modes propagating in flawed aluminum specimens with different grades of cross-sectional area loss. Dashed lines show the theoretical group velocity of each mode at a defect-free specimen.

As expected, the group velocity of the T(0,1) mode does not show any significant dependence on the cross-sectional area loss, although a slightly variation is observed. The group velocities within a defect-free pipe and a specimen with a full-circumferential defect are equal. But, those of specimens with partial-circumferential defects are smaller. In these specimens, the waves take a detour around the defect, causing a longer propagation distance resulting in a smaller group velocity.

For a T(0,2) mode generated, the observed group velocity at the defect varies depending on the cross-sectional loss. In the first four defective specimens with a smaller percentage of defective circumferences, the observed group velocity is smaller than that of a defect-free pipe (0%

cross-sectional loss). This is caused by a detour of the T(0,2) mode around the defect which causes a longer propagation distance. However, when the cross-sectional loss is around 35%, which corresponds to approximately one-half of the circumference, the group velocity suddenly increases. The group velocities in the rest of specimens with a larger defective circumference are relatively constant and close to that of T(0,1) mode. This result indicates the mode conversion from the T(0,2) mode to the T(0,1) mode at these defects.

Figure 4.3 shows the waveforms received by the R-EMAT when the T(0,2) mode is generated in specimens with approximately 25%, 60% and full-circumference defects. In the first specimen, the narrow defect does not cause mode conversion and the detected signal consists only of the generated T(0,2) mode. The observed waveform in this specimen is broader compared to the other two specimens. This is caused by the scattering from the defect when the waves are taking the detour around it. In the second specimen, the generated wave apparently splits into two waves. The first waves, marked with an asterisk, arrive earlier because it experiences mode conversion to the T(0,1) mode, which has a higher velocity at the defect. The second wave is the original T(0,2) mode. In the last specimen with a fully circumferential defect, the entire wave converts to the T(0,1) mode at the defect, resulting in a shorter traveling time. It can then be concluded that with the present configuration, the phenomenon of conversion to a higher mode can be a basis to detect a loss in pipe thickness that covers approximately one-half of its circumference.

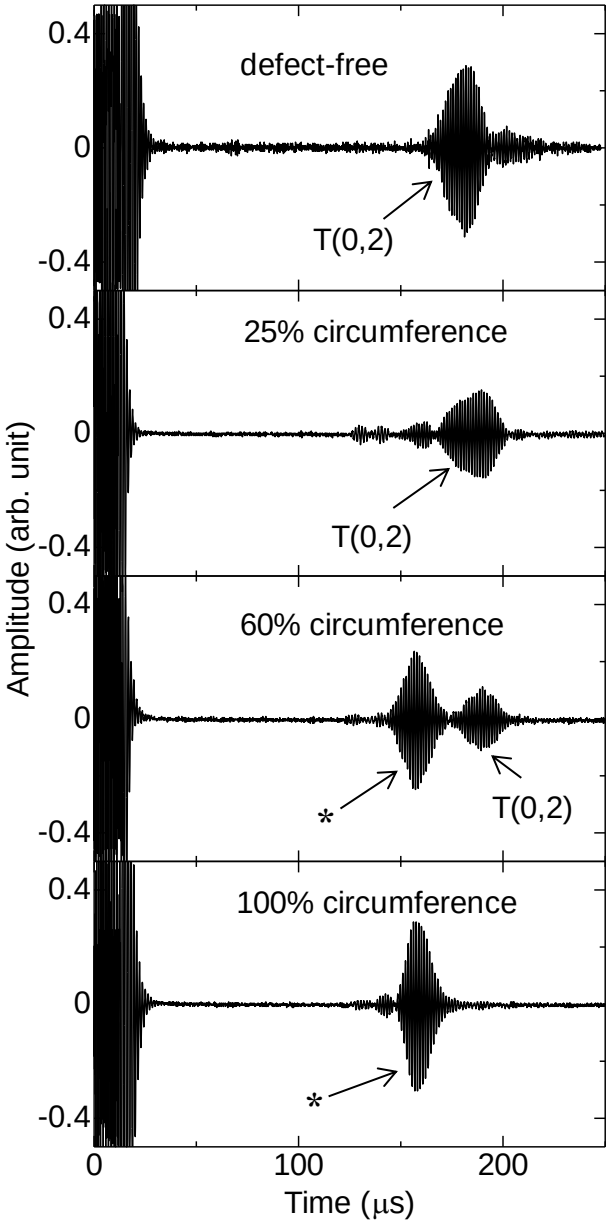

Figure 4.3 Received waveforms when T(0,2) mode is generated in specimens containing different percentages of circumferential defect. Signals with an asterisk are produces by conversion to T(0,1) mode at the defect [57].

b. Steel pipe

The behavior reported in the previous section should be independent of the type of material. For confirmation, an experiment is conducted with several steel pipes containing similar types of defects. The group velocity at a defect as a function of cross-sectional area loss percentage is shown in Fig. 4.4. Basically, the same results are obtained as those of the aluminum pipes. The group velocity of the T(0,1) mode generation is barely affected by the presence of a defect. Conversion of the generated T(0,2) to a T(0,1) mode is observed when the cross sectional loss is approximately 40% or more, indicated by a jump in group velocity.

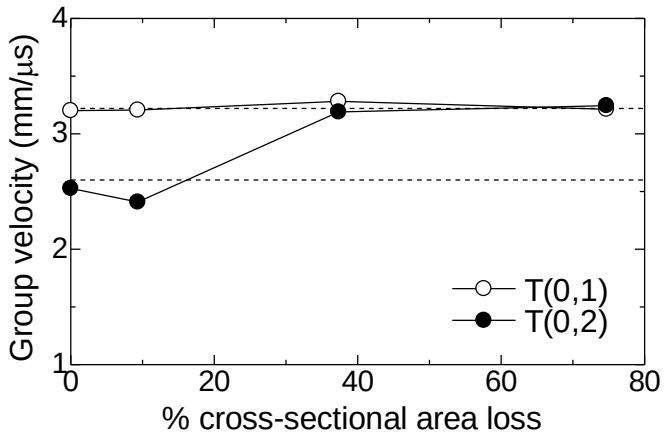

Figure 4.4 Group velocity at defects when the T(0,1) and T(0,2) modes are generated in defective steel pipes with different grades of cross-sectional loss. Dashed lines show the theoretical group velocity of each mode at a defect-free specimen.

4.2.2 Various axial length defects

The next outside inspection is to evaluate defects with different axial lengths. In all specimens, the defect covers the entire circumference with step-like edges. Remaining thicknesses at every defect is 1 mm, which is smaller than the cut-off thickness of the T(0,2) mode. As such, this mode should convert to T(0,1) mode at the defect. This experiment will then investigate the minimum length of defect that can induce conversion of the T(0,2) mode. Several steel pipe specimens containing defects are prepared. The T(0,1) and T(0,2) modes are generated by the transmitting EMAT and detected by the receiving EMAT. Figure 4.5 shows the placement of the two EMATs to the pipe, where a defect is located between them. In each specimen, several measurements are carried out to obtain the traveling time for different distances between the two EMATs, from which the average group velocity at the defect is obtained. The group velocity at a defect of different axial lengths is presented in Fig. 4.6. The horizontal axis is the axial length shown in a logarithmic scale. The two dashed lines correspond to the group velocities of these modes in a defect-free region (3.5-mm thick).

The observed group velocity of the T(0,1) mode at a defect is relatively constant at the same value as a defect-free specimen regardless of the varying lengths of defects. However, when the T(0,2) mode is generated, the observed group velocity is observed to be higher, close to that of a T(0,1) mode, indicating the conversion into this mode. The exception occurs when the defect's length is 2 mm. The observed group velocity at this defect is the same as that of a defect-free specimen, meaning that the mode conversion does not occur in this situation. The generated wave has a fixed wavelength of 5.22 mm which is determined by the periodicity of magnets arrangement, as shown by inset in Fig. 4.6. The conversion is observed when the length of defect is 5 mm or larger. It can then be concluded that the proposed method can be used to evaluate a defect which has comparable or longer than the wavelength of the probing wave.

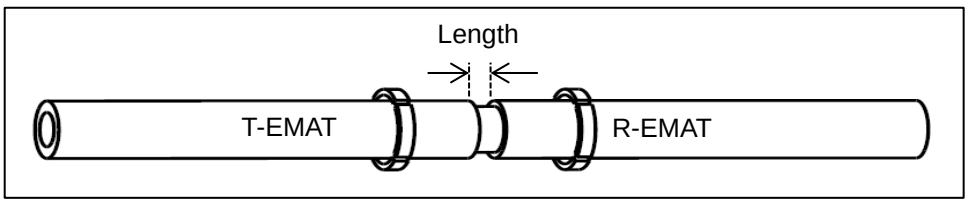

Figure 4.5 Pipe specimen with a defect and the placement of EMATs on it. The axial length of the defect is different in each specimen

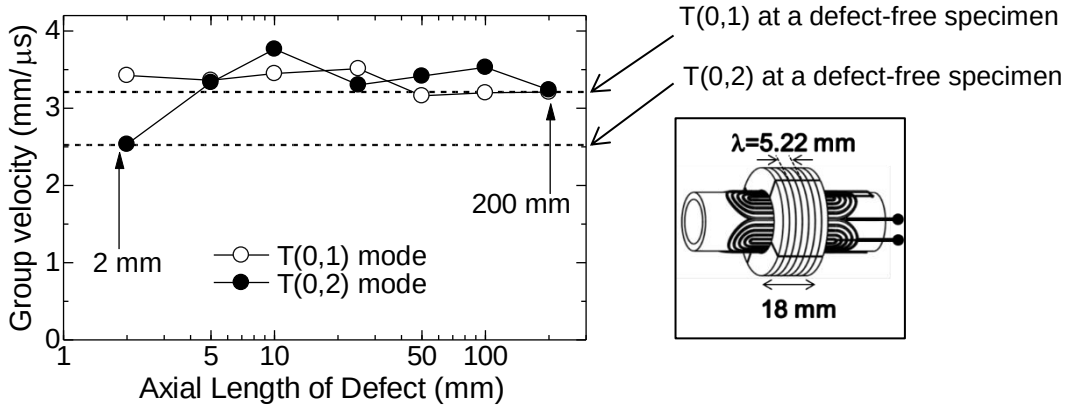

Figure 4.6 Group velocity at various defect's axial length. The horizontal axis is shown with a logarithmic scale. Inset shows the used EMAT.

4.3 Inside Inspection

Inspection from inside of the pipe is more preferable for actual applications. In many cases, the inspection can be done without stopping the operation. In addition, the pipe is usually covered or insulated in many cases, making an inspection from outside of the pipe not always practical. For that reason, an EMAT system to be used from inside should be developed. A fundamental study to observe the thickness dependence of group velocity is then performed. The developed system is also used to inspect steel pipes containing dish-shaped defects by using the group velocity change method.

4.3.1 EMAT's configuration

The system consists of a pair of identical EMATs as transmitter and receiver. The EMAT is constructed by an array of four PPM-EMATs as in the case of the external EMAT. There are six magnets in one PPM-EMAT. The periodicity between the magnets arrangement, hence the generated wavelength, is also 5.22 mm. Figure 4.7 shows a pair of EMAT as transmitter and receiver, and the configuration of such an EMAT. The two EMATs are placed around a steel rod, which assists in their movement from within the pipe. However this rod does not contribute to the electromagnetic-acoustic transduction process. The interaction between the eddy current produced by the current-carrying coil and the static magnetic field provided by the permanent

magnets generates the Lorentz force in the circumferential direction. This force leads to the acoustic vibration in that direction while the wave propagates in the axial direction. The lift-off between the EMATs and inside surface of the pipe is approximately 0.2 mm.

T(0,1) and T(0,2) modes are excited in a 3.5 mm thick steel pipe at frequencies of 0.60 and 0.78 MHz with experimental group velocities of 3.20 and 2.56 mm/μs, respectively. Figure 4.8 compares these experimental parameters with the calculated dispersion curves. The good agreement between these parameters confirms the ability of the developed EMAT to generate T(0,1) and T(0,2) modes. Figure 4.9 shows the typical propagating waveforms when the two modes are generated in a defect-free pipe. They are detected at 300 mm from the generating EMAT.

(a)

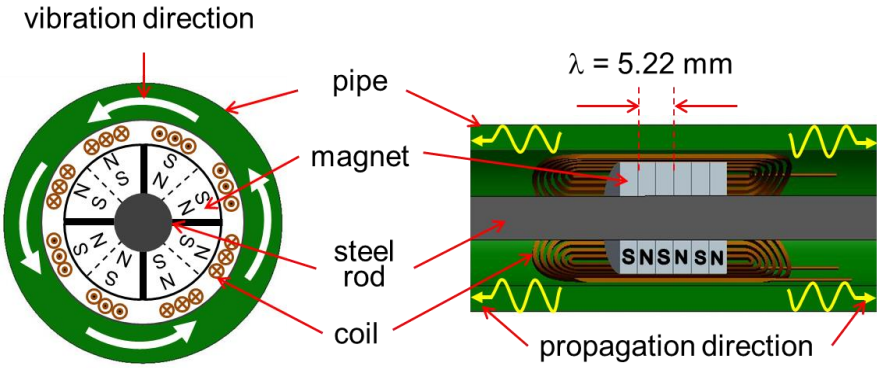

(b) (c)

(d)

Figure 4.7 Configuration of an EMAT for inspection from inside a pipe. (a) Placement of EMAT's pair inside the pipe, (b) cross-sectional view in the axial direction showing the involved fields to excite the Lorentz force, (c) side cross-sectional view showing the PPM arrangement, and (d) picture of one of the EMATs.

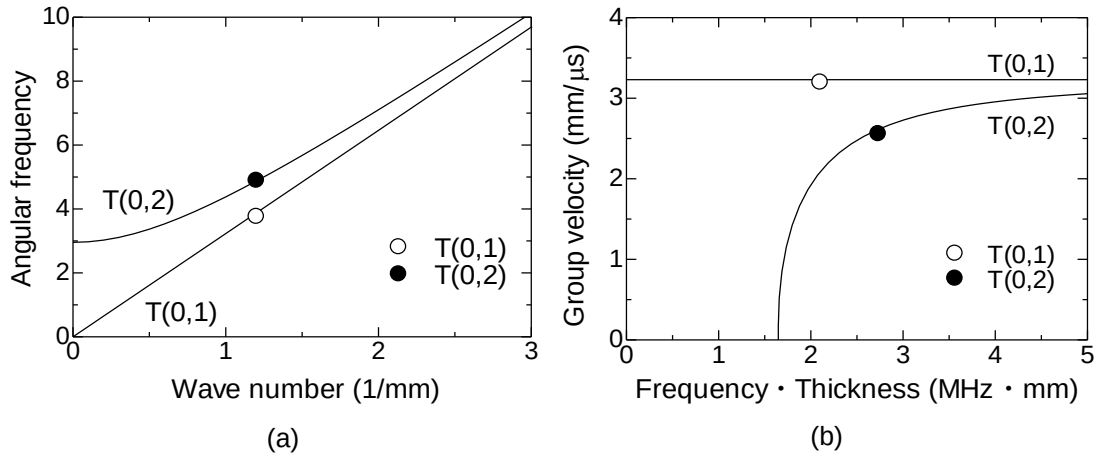

Figure 4.8 Comparison between the experimental parameters and the calculated dispersion curves for frequency (a) and group velocity (b).

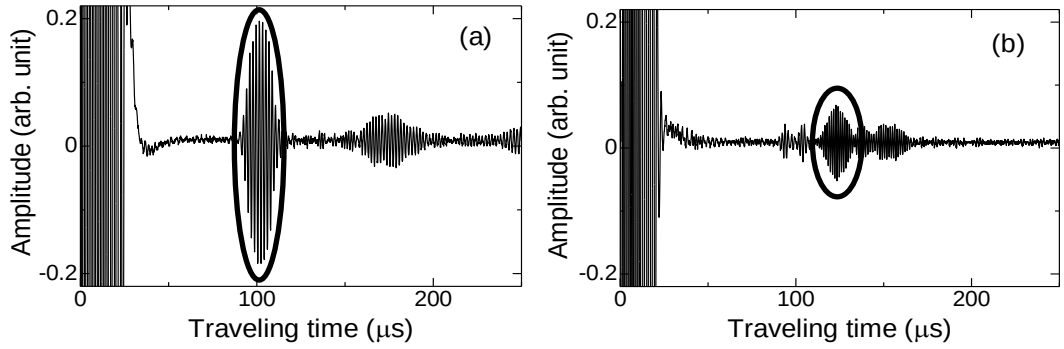

Figure 4.9 Typical received waveforms for the T(0,1) mode (a) and T(0,2) mode generations in a defect-free pipe. The intended signals are indicated by oval marks.

4.3.2 Thickness dependence of group velocity with inside EMATs

The investigation to observe the thickness dependence of group velocity is repeated with the current EMAT system for inspection performed from inside a pipe. The specimens for this experiment are the same as those used in section 3.4.3. Figure 4.10 presents the observed traveling times and comparison of the actual group velocities at the defect and the dispersion curves for the T(0,1) and T(0,2) modes in these specimens. Inspection from inside of the pipe successfully reproduces the same results as those made with an outside measurement reported earlier. Group velocity of the T(0,1) mode at the defect seems unaffected by the presence of defects with different depths, due to the non-dispersive characteristic.

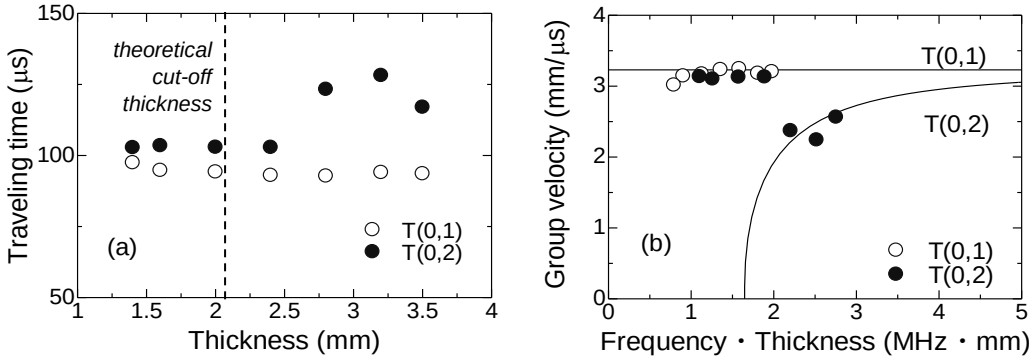

Figure 4.10 Observed traveling time (a) and group velocity dependence on the remaining thickness (b) of torsional modes in steel pipes measured from inside the pipes, compared with the theoretical dispersion curves.

In the first three specimens with shallow defects, the observed group velocity of the T(0,2) mode decreases as the thickness decreases. It suddenly increases however in the fourth specimen with deeper defect (2.4 mm remaining thickness). Its group velocity is close to that of the T(0,1) mode, indicating a conversion to this mode. The group velocities in the rest of specimens with even deeper defects are relatively constant and close to those of the T(0,1) mode. The discrepancy between the theoretical and actual cut-off thickness is also observed here, which is probably caused by measurement error. This fundamental study shows the potential to apply this group velocity change behavior for inline inspection of a pipe.

4.3.3 Evaluation of dish-shaped defects

In this section, the developed internal EMAT system with group velocity change method is used to evaluate steel pipe containing a dish-shaped defect. This type of defect is commonly found, which is usually caused by pitting corrosion or mechanical contact with foreign objects. The defect is fabricated at the center of the pipe with a length in the axial direction of 27.8 mm. Remaining thickness at the deepest part of the defect is 1 mm which is smaller than the cut-off thickness of the T(0,2) mode. Figure 4.11 illustrates the part of the specimen where the defect is machined. The circumferential length is changed step by step such that the loss in cross-sectional area is different in each measurement. All the defects are made in the same location on the same pipe. The EMAT system is placed inside the pipe with the defect located between them. All measurements with different sizes of defect are done without removing the systems, i.e., the EMATs are kept inside the pipe during the defect fabrication. Distance between the transmitting and receiving EMAT is 300 mm. The fabrication and measurement are started

with the smallest defect of 15 mm circumferential, which causes cross section area loss of 11%. Then a larger defect is made at the same location and the next measurement is performed. This procedure is repeated until the largest defect, that causes 21% cross section area loss, has been measured. The T(0,2) mode is generated in the specimen containing each defect and the propagating time is attained. Measurement in a defect-free specimen is used to determine the actual group velocity at the defect-free section of the pipe. The traveling time of only at the pipe section containing a defect is then obtained. Because the axial length of a defect is known, the group velocity at this section can be determined. Figure 4.12 presents the observed group velocity at the defect with different cross-sectional losses.

The dependence of group velocity on the percentage of cross-sectional loss is observed. The amount of cross-sectional loss corresponds to the converted portion of the generated T(0,2) mode to the T(0,1) mode. The increase in group velocity is observed as the cross-sectional loss increases because the area under the cut-off thickness also increases, causing a larger contribution of conversion to the T(0,1) mode with a higher velocity. When the cross-sectional area loss reaches 21%, the group velocity suddenly jumps close to that of the T(0,1) mode. In this case, the defect covers almost one-half of the total circumferences. The group velocity at even larger defects will be constant at those of T(0,1) mode.

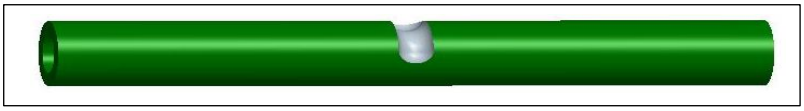

Figure 4.11 Steel pipe specimen containing a dish-shaped defect.

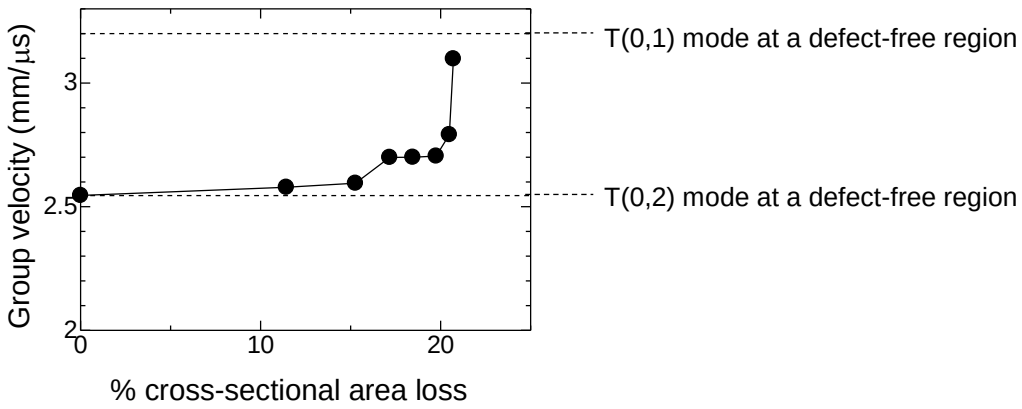

Figure 4.12 Group velocity at pipe section containing defects of the T(0,2) mode generated, showing dependency on the amount of cross-sectional area loss.

4.4.4 Scanning over multiple dish defects

The developed internal EMAT system is used to evaluate a steel pipe containing multiple dish-shaped defects to simulate a service scenario of pipe inspection. Dish-shaped defects of various sizes are fabricated in a specimen. The EMAT system is moved inside the pipe by manually pulling the suspension shaft from outside. Figure 4.13 illustrates a side-cross-sectional view of the pipe showing the placements of EMATs and the defects. The two EMATs are separated by 150 mm. Total length of the pipe is 1000 mm and the first defect is about 100 mm from the edge while the second one is located at the center. The system continuously measured the amplitude and phase of the generated T(0,2) mode while being translated from left to the right in the axial direction to perform a scanning measurement.

Measurement results are shown in Fig. 4.14. It shows the relative phase and amplitude which are normalized to those obtained at a defect-free region. The data is attained at every 10 mm in the axial direction. The point of measurement corresponds to the center between the two EMATs. The thickness profile at the pipe-wall is also added on top of the figure, showing the location of the defects. The phase obtained at the location of the defects is apparently shifted from that at the defect-free region. Near the end of the pipe, the magnetic field produced by the permanent magnets of the EMATs has a different profile than that of in the middle. Red dots are the phase response at the associated measurement point, without the presence of defect. The profile near the end of the pipe is apparently different than that of at the middle. The phase response of the first defect is affected by this, causing a more complicated behavior when compared to the second defect. The span of which the phase shift occurs equals to the distance between the two EMATs; therefore it is wider than the defect itself. On the other hand, the presence of defects does not directly influence the amplitude response. It can be concluded that the phase measurement, which is related to velocity, of the T(0,2) mode shows a potential to be used as a tool for defect detection and characterization

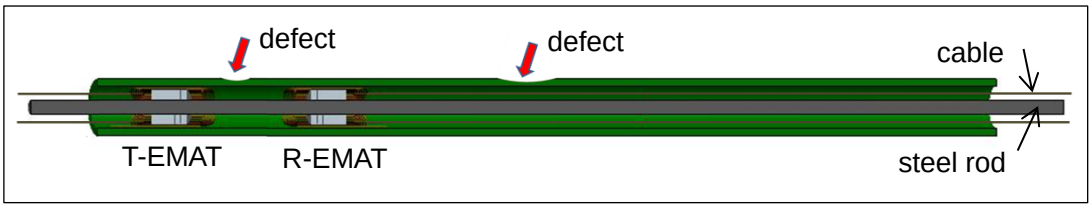

Figure 4.13 Internal EMATs' placement in the pipe and the location of defects.

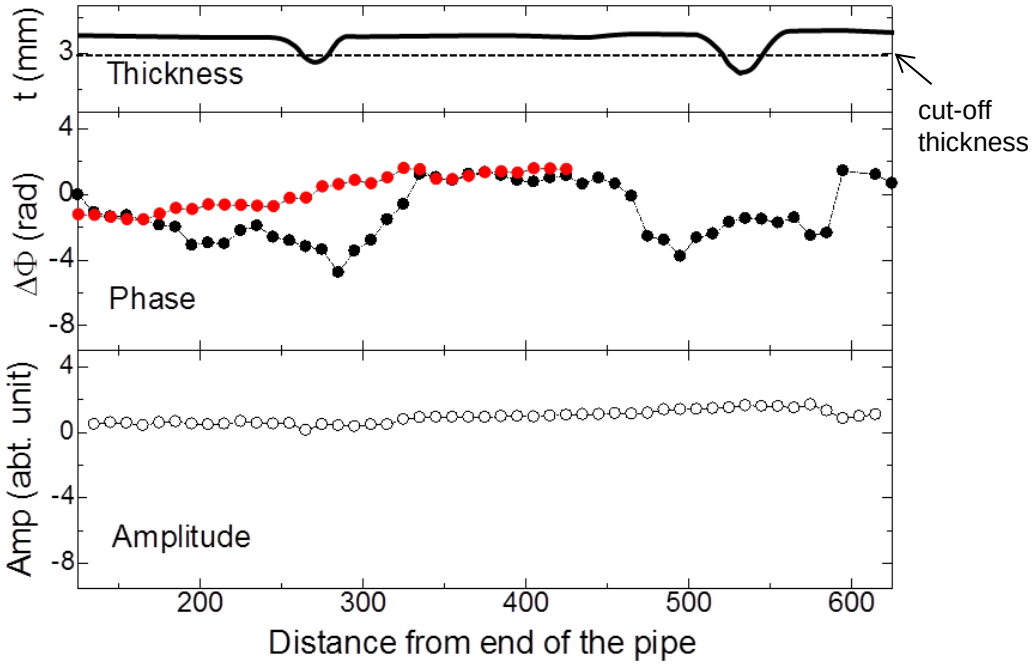

Figure 4.14 Axial scanning data showing phase shift and amplitude of the T(0,2) mode. Red dots indicate the measured phase at the associated measurement points in absence of defect. Thickness profile of the pipe-wall and the cut-off thickness of the T(0,2) mode are also shown.

CHAPTER V

SUMMARY AND CONCLUSIONS

Pipe structures are extensively used in industrial applications, many of which involve the transportation of flammable material at a high pressure. Any failure in this infrastructure could lead to a serious disaster. Integrity of the structure must always be of the highest importance; ergo, regular inspection is indispensable. Wall thinning (metal loss) is one of the primary vectors of pipe rupture. Pipe inspection by means of ultrasonic guided waves offers a fast-screening examination of the entire through-thickness and length of pipe. Inspection across a wider inspection area can be done in a one-time measurement. The common method to generate the guided waves in the specimen depends on contact piezoelectric transducer. The necessity of an intimate contact with the object structure often limits the application in many situations. The currently practiced inspection with ultrasonic guided waves is based on reflected amplitude from the defect. Intensity and stability of the signal is substantial in this method –something that is not always easy to get.

In the present study, a new approach to guided wave inspection was proposed. The proposed method is based on measuring group velocity change of torsional waves induced by mode conversion at the sites of pipe wall thickness change. This method relies on the measurement of traveling time – something less dependent on signal strength, in contrast with the more common amplitude-based method. Signal strength is highly affected by the background noise and contacting condition. Thus, this method would then provide a more reliable inspection. The Group velocity change method is possible to be applied with torsional guided waves due to the simple dispersion characteristic. In addition, torsional waves can propagate far greater distances than the other guided waves and tolerate the presence of insulator, which commonly surrounds the pipes in many applications. In the proposed method, the operating frequency must be fixed during the inspection. This is realized by using custom designed and fabricated electromagnetic acoustic transducers (EMATs). This is an entirely noncontact transducer, enabling measurement even at high temperatures; less physical site preparation needed prior to inspection, and reduces time required for inspection itself.

Chapter II briefly introduced the torsional guided wave and its dispersion behavior. It gave the basic principle from which the proposed inspection method was derived. The existence of the so-called “cut-off thickness” of higher torsional modes was familiarized. This chapter also mentioned several available methods to generate this wave. The EMAT was introduced and the summary of its generation/detection mechanism was given. Configuration of the original design for the current EMAT was explained. A pair of identical EMATs was used as transmitter and receiver to generate the fundamental and higher modes of torsional waves. The fundamental T(0,1), the second and third higher T(0,2) and T(0,3) modes were generated in an aluminum pipe while the T(0,1) and T(0,2) modes were generated in a steel pipe. The optimum frequency and group velocity of each mode obtained by experiment had good agreement with the theoretical dispersion curves.

Some fundamental studies exploring the propagation and mode conversion behavior of torsional guided waves were presented in Chapter III. An investigation of group velocity dependence on thickness was performed by measuring propagation times across known distances of several specimens containing defects. The observed group velocity of the T(0,2) mode was highly influenced by the remaining thickness at the defect. When the defect was shallow, the group velocity decreased as the thickness decreased, following the theoretical dispersion curve smoothly. In specimens with deeper defects, where the remaining thickness was smaller than the cut-off thickness, the group velocity suddenly jumped, being equal to that of the T(0,1) mode. This result indicated a conversion of the generated T(0,2) mode to a T(0,1) mode. The group velocities in the specimens with even smaller remaining thicknesses remained at comparable values with those that belong to the T(0,1) mode. The experimental group velocity of the T(0,1) mode generated was independent of the thickness and no significant variation was observed. This result confirmed the non-dispersive characteristic of the fundamental T(0,1) mode. The experiment was done both in aluminum and steel pipe specimens and similar results were attained.

In order to investigate the detailed mechanism of this conversion, further experimentation was carried out. A torsional mode was generated in a specimen containing a deep defect which caused the remaining thickness to be smaller than the cut-off thickness of the T(0,2) mode. The propagating waves were detected point by point in the axial direction and the traveling time at each point was obtained. The relationship between the distance and traveling time at many measurement points was obtained, which was inversely proportional to the group velocity. It is understood that the generated T(0,1) mode continued propagating at the defect, while it converted to the higher T(0,2) mode after the defect. This investigation revealed that the

generated T(0,2) mode converted to the T(0,1) at the defect, and reconverted after the defect when the thickness returned to the original value. This mechanism of mode conversion was experimentally observed for the first time.

Influence over conversion behavior at a defect's edge was also investigated. The two modes were propagated in several defective specimens with gradual thickness transitions at the edges of defects. The T(0,1) mode was less reflected at the leading edge as the thickness change was smoother. Conversion to a higher mode was not observed after the defect. The slope of the thickness transition affected the T(0,2) mode in the opposite way. More reflection from the edge was observed as the thickness transition was smoother. In a specimen containing a tapered defect with a very smooth thickness transition at the edge, the T(0,2) mode was totally reflected in the sloping region of the edge. There was no transmitted wave through the defect. The total reflection point corresponded to the cut-off thickness of this mode. This is a very intriguing discovery which was also observed for the first time. Considering the rarely reported experimental work on torsional waves, the phenomena investigated in this chapter will certainly contribute to the basic science as well as be beneficial for industrial application.

To verify its practical application, the inspection by torsional waves was performed from inside of a sample pipe. An EMAT system for inside inspection was then developed which consisted of a pair of identical EMATs placed around a steel rod. The rod was used as a shaft to help the placement and movement of the EMATs through the pipe. Chapter IV reported some applications of the proposed method to inspect various cases of defective aluminum and steel pipes both by outside and inside inspection methods.

External inspection was performed on several pipes containing circumference partial defects, *i.e.* the defects did not cover the entire circumference of the pipe. The defect in each specimen had a different length in the circumferential direction, which gave a different cross-sectional area loss. In the specimen containing a partial circumferential defect, the T(0,1) mode tended to take a detour around the defect, causing a longer propagation distance, hence a smaller observed group velocity. The similar behavior was observed when the T(0,2) mode was propagated in specimens containing defects which caused 20% or less cross-sectional loss. The detour of the waves caused a smaller group velocity. However, when the cross-sectional loss is larger than 20%, the obtained group velocity of the T(0,2) mode generated suddenly jumped up, comparable to that of the T(0,1) mode. It can be concluded that the conversion of T(0,2) to T(0,1) mode occurred even when the thinning region did not cover the entire circumference of the pipe.

An experiment to investigate the minimum detectable axial length of a defect was also performed. Several specimens containing different length of defects were inspected. The observed group velocity at defect of the T(0,2) generation was higher when the length was 5 mm or more. It was comparable to that belongs to the T(0,1) mode, again indicating a conversion to this mode. However, when the length was 2 mm, the observed group velocity was equal to the generated T(0,2) mode. Since the generated wavelength was 5.22 mm, it can be concluded that mode conversion occurred when the length of a defect was comparable with the wavelength or longer.

The T(0,2) mode was used to examine specimens containing dish-shaped defects by using the internal-EMAT system. This is a commonly found, serious type of defect, which can be caused by corrosion. Various sizes of defects, resulting in different amounts of cross-sectional area loss, were fabricated in a steel pipe specimen. The observed group velocity increases as the loss increases, showing a higher converted portion of the generated T(0,2) to a T(0,1) mode. A group velocity jump, indicating a conversion to a T(0,1) mode, was observed when the loss reached approximately 22% of the total cross section area

Lastly, an experiment was performed to simulate a service scenario of a pipe inspection. The T(0,2) mode was generated and detected by the internal-EMAT system and used to inspect a steel pipe containing multiple defects of various depths machined at different axial positions. The EMAT system was moved inside the pipe by manually pulling the suspension shaft from outside. The system continuously measured the amplitude and phase while being translated along the pipe to perform a scanning measurement. The phase attained at the location of the defects was apparently shifted from those obtained throughout the defect-free region, successfully indicating the presence of defects. Furthermore, with a very careful measurement, different sizes of defect would cause a different phase response, potentially enabling the ability to size and characterize the individual defects. For practical applications, the suspension shaft should be made from a flexible material. This would enable the system to inspect not only a straight but also a curved pipe. An automatic system to help and control the movement inside the pipe will be also advised. For an even more advance application, the system can be installed in a pig measurement tool which follows the fluid stream along the pipe.

To conclude, non-contact EMAT system for fundamental and higher torsional modes generation have been successfully developed, both for external and internal pipe inspections, and the various investigations performed in the present study confidently show the applicability of the group velocity change method for pipe inspection.

REFERENCES

1. C. J. Hellier, Handbook of Nondestructive Evaluation, (McGraw-Hill, New York, 2011).
2. J.D Achenbach (2000). Quantitative Nondestructive Evaluation, *International Journal of Solid and Structure, 37*, p. 13.
3. G. Dobmann (2006), Magnetic NDT Technology for Characterizing Materials – A State of the Art Survey, Proceeding of National Seminar on Non-Destructive Evaluation Dec. 7 - 9, 2006, Hyderabad.
4. H. Kriesz (1979), Radiographic NDT – A Review, *NDT International, December 1979*, p. 270.
5. X. Zhu, *et al*. (2010), Ultrasonic Guided Waves for Nondestructive Evaluation/Structural Health Monitoring of Trusses, *Measurement Science and Technology, 21*, p. 12.
6. G.Y. Tian (2005), Defect classification Using New a Feature For Pulsed Eddy Current Sensors, *NDT & E International, 38, Issue 1,* p. 77..
7. A. N. Ser'eznov, *et al*. (2008), Acoustic- Emission Testing of Curvilinear Fuselage Panel of an RRJ Airplane in Life, *Russian Journal of Nondestructive Testing, 44,* p. 836.
8. M. Hirao and H. Ogi, EMATs for Science and Industry: Noncontacting Ultrasonic Measurements (Kluwer Academic Publisher, Boston/Dordrecth/London, 2003).
9. Pipeline Accident Report: Rupture of hazardous liquid pipeline with release and ignition of propane, Carmichael, Mississippi, November 1, 2007. National Transportation Safety Board (2009).
10. Pipeline Accident Report: Pacific gas and electric company natural gas transmission pipeline rupture and fire, Sun Bruno, California, September 9, 2010. National Transportation Safety Board (2011).
11. F. Hasan, *et al*. (2007), Stress Corrosion Failure of High-Pressure Gas Pipeline, *Engineering Failure Analysis, 14,* p. 801.
12. Z. A. Majid, *et al*. (2010), Failure Analysis of Natural Gas Pipes, *Engineering Failure Analysis, 17*, p. 818.
13. X.B. Li, *et al*. (2009), Numerical Simulation and Experiments of Magnetic Flux Leakage Inspection in Pipeline Steel, *Journal of Mechanical Science and Technology, 23*, pp. 109.
14. Y. Sun, *et al*. (2010), A New MFL Principle and Method Based on Near-Zero Background Magnetic Field, NDT*&E International, 43*, p. 348.
15. J. Atzlesberger, *et al*. (2010), Magnetic Flux Leakage Measurement Setup for Defect Detection, *Procedia Engineering, 5*, p. 1401.

16. W. Cheng (2012), Pulsed Eddy Current Testing of Carbon Steel Pipes' Wall-thinning Through Insulation and Cladding, *Journal of Nondestructive Evaluation, 31*, p. 215.
17. J.B. Nestleroth, *et al*. (2007), Application of Eddy Currents Induced by Permanent Magnets for Pipeline Inspection, *NDT&E International, 40*, p. 77.
18. Z. Xu, *et al*. (2012), Assessment of Wall Thinning in Insulated Ferromagnetic Pipes Using the Time-to-Peak of Differential Pulsed Eddy-Current Testing Signals, *NDT&E International, 51*, p. 24.
19. J.L. Rose, *et al*. (1994), A Guided Wave Inspection Technique for Nuclear Steam Generator Tubing, *NDT&E International, 27*, p. 307.
20. M.J.S. Lowe, *et al*. (1998), Defect Detection in Pipes Using Guided Waves, *Ultrasonics, 36*, p. 147.
21. J.L. Rose: Ultrasonic Waves in Solid Media (Cambridge University Press, Cambridge, 1999) Chap. 12.
22. H.J. Shin, *et al*. (1999), Guided Waves by Axisymmetric and Non-Axisymmetric Surface Loading on Hollow Cylinders, *Ultrasonics, 37*, p. 355.
23. J.L. Rose, Ultrasonic Guided Waves in Structural Health Monitoring, *Key Engineering Material, 14*, p. 270.
24. X. Wang, *et al*. (2010), Experimental Investigation of Reflection in Guided Wave-Based Inspection for the Characterization of Pipeline Defects, *NDT&E International, 43*, p. 365.
25. H. Sato, *et al*. (2010), Theoretical and Simulated Analysis of Guided Waves Propagating in Fluid-Filled Pipes, *Japanese Journal of Applied Physics, 49,* 07HC08.
26. H. Kwun, *et al*. (2005), Reflection of the Fundamental Torsional Wave from a Stepwise Thickness Change in a Pipe, *Journal of Korean Physics Society, 46,* p. 1352.
27. Y.Y. Kim, *et al*. (2005), Torsional Wave Experiments with a New Magnetostrictive Transducer Configuration, *Journal of Acoustic Society of America, 117*, p. 3459.
28. S.H. Cho, *et al*. (2006), Noncontact Torsional Wave Transduction in a Rotating Shaft Using Oblique Magnetostrictive Strips, *Journal of Applied Physics, 100*, 104903.
29. F. Blum, *et al.* (2005), A Focused Two-Dimensional Air-coupled Ultrasonic Array for Non-Contact Generation, *NDT&E Internationa*l, *38*, p. 634.
30. W. Ke, *et al.* (2009), 3D Finite Element Simulations of an Air-Coupled Ultrasonic NDT System, *NDT&E International, 42*, p. 524.
31. T. Watanabe, *et el.* (2002), Ultrasonic Excitation by Phase Velocity Scanning of Laser Beam and Application to Nondestructive Evaluation, *Japanese Journal of Applied Physics, 41*, p. 3547.
32. C. E. Duffer, *et al*. (1996), Narrow Band Laser Ultrasonic NDE, *Review of Quantitative Nondestructive Evaluation, 15*, p. 593.

33. R. B. Thompson (1990). Physical Principles of Measurements with EMAT Transducers. In: Thurston, R.N., Pierce, A.D. (Eds.), Ultrasonic Measurement Methods, Physical Acoustics, vol. XIX. Academic Press, p. 157.
34. JL. Rose, *et al.* (1997), Laser Based, Guided Wave Experiments for Tubing, *Experimental Mechanics, 37*, p. 165.
35. M. Hirao, *et al*. (1999), An SH-wave EMAT Technique for Gas Pipeline Inspection, *NDT&E International, 32*, p. 127.
36. Nurmalia, *et al*. (2011), Detection of Shear Horizontal Guided Waves Propagating in Aluminum Plate with Thinning Region, *Japanese Journal of Applied Physics, 50*, 07HC17.
37. Nurmalia, *et al*. (2011), Mode Conversion Behavior of SH Guided Wave in a Tapered Plate, *NDT&E International, 45*, p. 156.
38. S. A. Uribe, *et al*. (2009), Mode Conversion of SH Guided Wave at Defects for Pipeline Inspection, *Review of Quantitative Nondestructive Evaluation, 28B*, p. 1550.
39. H. Nishino, *et al*. (2001), Modal Analysis of Hollow Cylindrical Guided Waves and Applications, *Japanese Journal of Applied Physics, 40*, p. 364.
40. Demma, *et al*. (2003), The Reflection of the Fundamental Torsional Mode from Cracks and Notches in Pipes: *Journal of Acoustic Society of America, 114*, p. 611.
41. A. Lovstad, *et al*. (2011), The Reflection of the Fundamental Torsional Guided Wave from Multiple Circular Holes in Pipes, *NDT&E International, 44*, p. 553.
42. A. Lovstad, *et al*. (2012), The Reflection of the Fundamental Torsional Mode from Pit Clusters in Pipes: *NDT&E International, 46*, p. 83.
43. H.E. Engan (1998), Torsional Wave Scattering from a Diameter Step in a Rod, *Journal of Acoustic Society of America, 104*, p. 2015.
44. H.E. Engan (1999), Torsional Rod Wave Scattering from Tapering Between Regions of Diferent Cross-Sections, *IEEE Transaction on Ultrasonics, Ferroelectrics and Frequency Control, 46*, p. 1035.
45. R. Kirby, *et al.* (2012), On the Scattering of Torsional Elastic Waves from Axisymmetric Defects in Coated Pipes, *Journal of Sound and Vibration, 331*, p. 3989.
46. H. Nishino, *et al.* (2010), Long-Range Testing of Welded Elbow Pipe Using the T(0,1) Mode Ultrasonic Guided Wave, *Japanese Journal of Applied Physics, 49*, 116602.
47. H. Nishino, Experimental Investigation of Mode Conversions of the T(0,1) Mode Guided Wave Propagating in an Elbow Pipe, *Japanese Journal of Applied Physics*, 50, 046601.
48. D. C. Gazis, (1958), Exact Analysis of the Plane-Strain Vibrations of Thick-Walled Hollow Cylinders, *Journal of Acoustic Society of America, 30*, p. 786.
49. T. R. Meeker, *et al.* (1964), Guided Wave Propagation in Elongated Cylinders and Plates, in Physical Acoustic I, Academic Press., New York/London.

50. H. Kolsky, Stress Waves in Solids (Dover Publication, New York, 1963), Chap. 3.
51. J. O. Kim, *et al.* (2003), Vibration Characteristics of Piezoelectric Torsional Tansducers, *Journal of Sound and Vibration, 264*, p. 453.
52. H. Ogi (1997), Field Dependence of Coupling Efficiency between Electromagnetic Field and Ultrasonic Bulk Waves, *Journal of Applied Physics, 82*, p. 3940.
53. R. Ribichini, *et al.* (2012), The Impact of Magnetostriction on the Transduction of Normal Bias Field EMATs, *NDT&E International, 51*, p. 8.
54. F. Vasile, *et al.* (1979), Excitation of Horizontally Polarized Shear Elastic Waves by Electromagnetic Transducers with Periodic Permanent Magnets, *Journal of Applied Physics, 50*, p. 2583.
55. Nurmalia, *et al.* (2012), Mode Conversion of Torsional Waves Generated by Electromagnetic Acoustic Transducer, *Review of Quantitative Nondestructive Evaluation, 32*, p. 909.
56. Nurmalia, *et al.* (2013), Mode Conversion and Total Reflection of Torsional Waves for Pipe Inspection, *Japanese Journal of Applied Physics, 52*, 07HC14.
57. K. A. Macdonald, *et al*. (2007), Assessing Mechanical Damage in Offshore Pipelines –Two Case Studies, *Engineering Failure Analysis, 14*, p. 1667.
58. R. Caradente, *et al*. (2010), The Scattering of the Fundamental Torsional Mode from Axi-symmetric Defects with Varying Depth Profile in Pipes, *Journal of Acoustic Society of America, 127*, p. 3440.

ACKNOWLEDGMENT

Completion of this thesis is impossible without great guidance, advices and supports from many people. I would like to express my deepest gratitude to the following person.

- Prof. M. Hirao, the Head Professor of Hirao Laboratory, Graduate School of Engineering Science, Osaka University, for his countless kindness, started from trusting me with the opportunity to join this great laboratory to his endless support and encouragement.
- Associate Prof. H. Ogi of Hirao Laboratory, Graduate School of Engineering Science, Osaka University, for his valuable advices and constructive opinion throughout my study.
- Assistant Prof. N. Nakamura of Hirao Laboratory, Graduate School of Engineering Science, Osaka University for his guidance and kind encouragement. Working under his direct supervision inspires me the spirit of perfection in work.
- Mr. K. Yaegawa, a former technician at Hirao Laboratory, Graduate School of Engineering Science, Osaka University for his support and kindness, despite the communication difficulty due to my Japanese problem.
- Academic and administrative staffs of Graduate School of Engineering Science, especially Department of Mechanical Science and Bioengineering for the support.
- Mr. M. Nishiyama of Central Workshop, Osaka University for helping me with the specimens.
- Assistant Prof. K. Tanigaki of Kobayashi Laboratory who is also a kind senior at Hirao Lab for being a supportive senior.
- Mr. Tyler LeBrun for his support and encouragement. Good luck for your turn.
- Students of Hirao Laboratory, a group of young people who always try to give their best in everything. Salute.
- People at Sigma International Students Center for the nice friendship.
- The big family of Indonesian Students Association for being a home in Japan.
- Love and foremost thanks to my parent and family for their everlasting supports and prayers.

Last but not the least; I have to express my gratitude to the Ministry of Education, Culture, Sports and Technology of Japan, Graduate School of Engineering Science, Osaka University, for providing me an opportunity to do this research. Hopefully this little work can contribute to the prosperity of mankind.

PUBLICATIONS

1. Nurmalia, Nobutomo Nakamura, Hirotsugu Ogi and Masahiko Hirao, Mode conversion and total reflection of torsional waves for pipe inspection, *Japanese Journal of Applied Physics*, Vol. 52, 07HC14, July, 2013.
2. Nurmalia, Nobutomo Nakamura, Hirotsugu Ogi and Masahiko Hirao, Mode conversion of torsional waves generated by electromagnetic acoustic transducer, *AIP Conf. Proc.*, Vol. 1511, Review of Progress in Quantitative Nondestructive Evaluation QNDE2012, pp. 909 – 915, 2013.
3. Nurmalia, Nobutomo Nakamura, Hirotsugu Ogi, Masahiko Hirao and Kazuyuki Nakahata, Mode conversion behavior of SH guided wave in a tapered plate, *NDT&E International*, Vol. 45, pp. 156 – 161, January, 2012
4. Nurmalia, Nobutomo Nakamura, Hirotsugu Ogi and Masahiko Hirao, Detection of shear horizontal guided waves propagating in aluminum plate with thinning region, *Japanese Journal of Applied Physics*, Vol. 50, 07HC17, July, 2011.

CONFERENCES

1. International Congress on Ultrasonics 2013, May 2013, Singapore (oral presentation).
2. Symposium on Ultrasonic Electronic USE2010, November 2012, Chiba, Japan (poster presentation).
3. Review of Progress in Quantitative Nondestructive Evaluation QNDE2012, July 2012, Denver Tech Center, Colorado, USA (oral presentation).
4. Review of Progress in Quantitative Nondestructive Evaluation QNDE2011, July 2011, Burlington city, Vermont, USA (oral presentation).
5. Symposium on Ultrasonic Electronic USE2010, December 2010, Tokyo, Japan (oral presentation).
6. Mechanical Engineering Congress 2010, September 2010, Nagoya Japan (oral presentation).

AWARD

Young Scientist Award, Symposium of Ultrasonic Electronic USE2010